Scientific Reports

https://doi.org/10.1038/s41598-026-43070-1

Article in Press

Green-synthesized *N*-acetylcarnosine–loaded gold nanoparticles as a novel ocular nanocarrier for antioxidant therapy and cataract prevention

Received: 23 January 2026

Accepted: 28 February 2026

Published online: 24 March 2026

Cite this article as: Abid A.S., Al-Garawi Z.S. & Öztürkkan F.E. Green-synthesized *N*-acetylcarnosine–loaded gold nanoparticles as a novel ocular nanocarrier for antioxidant therapy and cataract prevention. *Sci Rep* (2026). https://doi.org/10.1038/s41598-026-43070-1

Ahmed Salih Abid, Zahraa S. Al-Garawi & Füreya Elif Öztürkkan

"Green-Synthesized N-Acetylcarnosine–Loaded Gold Nanoparticles as a Novel Ocular Nanocarrier for Antioxidant Therapy and Cataract Prevention"

Ahmed Salih Abid[1, 2], Zahraa S. Al-Garawi[1], Füreya Elif Öztürkkan [3]

[1]Chemistry Department, Mustansiriyah University, Baghdad, Iraq, P.O. Box: 14022

[2]Ibn Al-Haitham Teaching Eye Hospital, Ministry of Health, Baghdad, Iraq

[3]Chemical Engineering Department, Faculty of Engineering and Architecture, Kafkas University, Kars-Türkiye

[*]All correspondence is sent to [1*]**:** z.mohsin@uomustansiriyah.edu.iq

Abstract

Cataract represents one of the leading causes of blindness worldwide and is primarily attributed to protein glycation, oxidative stress, and aggregation of lens crystallins. Surgical lens extraction remains the standard treatment, which, despite its effectiveness, carries potential postoperative risks and economic burdens, thereby underscoring the need for alternative, non-surgical therapeutic approaches. This study aimed to develop a green-synthesized nanosystem based on gold nanoparticles (AuNPs) using *Alchemilla vulgaris L.* (Lady's mantle) extract, aiming to achieve efficient antioxidant delivery and sustained therapeutic retention within ocular tissues. Gold nanoparticles were synthesized via the reduction of chloroauric acid ($HAuCl \cdot 3H_2O$) using the plant extract under ultrasonic agitation and dispersion, yielding AuNPs formulations 1%, 4%, and 7% (w/v). The synthesized nanocomposites were characterized using a UV–Vis spectroscopy, FTIR, XRD, FE-SEM, AFM, and zeta potential analysis. Bio activity was performed using DPPH radical scavenging, MTT assays for cytotoxicity testing, *in vitro* drug-release studies, and *ex-vivo* lens transparency assessments, all supported by computational molecular docking and ADMET (absorption, distribution, metabolism, and excretion) analyses .The results demonstrated that NAC-loaded gold nanoparticles (NAC–AuNPs) exhibited enhanced antioxidant activity, achieving 72% to 89% DPPH inhibition, and a high encapsulation efficiency of 86.1%. The drug-release profile exhibited a higher release rate observed under mildly acidic conditions (pH 6). *Ex-vivo* experiments using human cataractous lenses revealed a dose-dependent improvement in lens optical clarity at NAC concentrations of 0.05, 0.1, and 0.3 mM, loaded onto 7% (w/v) AuNPs formulations. Molecular docking studies suggested potential hydrogen-bond interactions between NAC and key lens crystallin proteins, providing mechanistic insight into possible structural stabilization of lens crystallin proteins. The green-synthesized AuNP–NAC nanosystem may represents a promising and biocompatible nanocarrier strategy that warrants further *in vivo* validation.

Keywords: Cataract; N-acetylcarnosine (NAC); Gold nanoparticles (AuNPs); Green synthesis; *Alchemilla vulgaris L.*; Antioxidant nanocarrier; Ocular drug delivery; Lens transparency; In-silico docking; Controlled release.

Introduction

Cataract is one of the leading causes of visual impairment and blindness worldwide and is characterized by the progressive opacification of the crystalline lens (1). Cataract contributes a significant percentage of moderate-severe vision loss in the entire world, especially in those who are above ≥50 years(2). Physiologically, lens transparency is maintained by the highly ordered organization of crystallin proteins and robust antioxidant defense mechanisms, but oxidative stress-induced reactive oxygen species (ROS), glutathione depletion, protein oxidation, and glycation gradually destabilize the system, eventually leading to crystallin aggregation and light scattering that ultimately result in cataractogenesis(3, 4).

Although surgical lens extraction is effective in restoring vision, it is an invasive procedure that carries post-operative risks, financial burdens, and limited availability in most areas (5). These restrictions have fuelled increased interest in non-surgical interventions to slow or prevent cataract development or progression by targeting underlying pathophysiological pathways rather than late lens opacification (6). Oxidative stress and protein glycation are some of these mechanisms that have been widely identified to be core processes in the destabilization and aggregation of lens proteins(7-10) .

Nanotechnology is a strong platform in ophthalmology, providing novel methods for diagnosis, imaging, and drug delivery in anterior and posterior segment eye diseases(11). The use of nanoparticle-based systems is especially appealing for ocular applications, as they allow overcoming precorneal loss, corneal permeability barriers, and rapid drug clearance, which considerably decrease the bioavailability of traditional eye-drop systems(8, 12-14) . In this regard, gold nanoparticles (AuNPs) have attracted significant interest due to their high biocompatibility, tunable size and surface chemistry, and unique optical properties(15, 16). AuNPs have proved useful not just in ocular imaging and photothermal therapy(17, 18), but also in general nanocarrier technology, with the capacity to increase ocular drug penetration, residence time, and release control(9, 10, 19-22) .

Since oxidative stress and protein aggregation play a key role in the development of cataracts, antioxidant-based therapy is a sensible non-surgical strategy for lens protection(23-26). But there is still a limitation in the clinical translation of such agents due to inefficient delivery to the eye and intraocular retention(8, 14). Nanocarrier-based delivery systems, especially AuNP-based systems, can provide a ray of hope for overcoming these obstacles by enhancing drug stability, improving drug permeability, and prolonging drug availability at ocular tissues (27, 28). In line with this, it is apparent that the creation of AuNPs-based antioxidant delivery systems is an interesting direction for the development of non-invasive interventions to slow the progression of cataract.

Yue Wang et al. demonstrated that Glutathione loss and a high level of oxidative stress have been shown to promote crystallin aggregation and damage lens transparency, thus increasing the cataract formation rate(10). On the same note, *P. Budnar et al*. found that age-associated post-translational alterations and protein misfolding trigger the formation of high-molecular-weight aggregates, which cause increased light scattering and lens opacification(27). Simultaneously, *Shehwaz Anwar et al*. demonstrated that the formation of crystallin cross-links and insoluble aggregates is caused by the buildup of advanced glycation end products (AGEs), and antioxidant substances

successfully inhibit oxidative and glycation-induced mechanisms and slow the development of cataracts(28). Although surgical lens replacement is the modern standard of care, it is invasive, expensive, and carries risks after the operation, which has contributed to interest in non-surgical pharmacological interventions(5, 6). In the same respect, N-acetylcarnosine (NAC) has been found by *U. Rodella et al*. to be a powerful antioxidant capable of alleviating oxidative stress in the lens microenvironment and maintaining lens transparency(29). The absence of effective clinical translation is, however, impeded by low ocular bioavailability; *G. Santos et al*. have indicated that less than 5 percent of topical ophthalmic drugs penetrate intraocular tissues through topical administration by reason of precorneal loss and restriction at the corneal barriers(30, 31). New solutions to these challenges are emerging with the development of nanotechnology. *G. Raiche et al*. showed that polyethylene glycol (PEG)-functionalized gold nanoparticles are highly stable and biocompatible in the eye(32). and *Ahmed et al*. demonstrated that antibody/peptide-functionalized AuNPs allow location-specific targeting(33). Notably, *Chen Y. et al*. reported that NAC loading onto AuNPs enhances ocular permeability and enables sustained antioxidant release(34), and *Manlin Qi et al*. confirmed that surface-functionalized AuNPs can penetrate the corneal layer without inducing cytotoxicity, supporting their suitability for advanced ophthalmic nanotherapies(35)

Cataract is the opacification of the crystalline lens, one of the major causes of vision impairment and blindness worldwide. Physiologically, lens transparency is ensured by antioxidant defensive systems and crystallin protein folding, but oxidative stress-induced crystallin modifications and protein aggregation enhance light scattering and lens opacification.

To illustrate the ability to induce a successful penetration of the ocular barriers, the current study proposed to create NAC loaded AuNPs (AuNPs-NAC) in order to improve ocular drug delivery and extend intraocular drug retention by controlled release by optimizing key physicochemical parameters such as particle size, surface charge, and functionalization to achieve a successful penetration through the ocular barriers.

Alchemilla vulgaris L .was chosen as the main plant material for this study because of its established phytochemical profile and proven antioxidant qualities. *Alchemilla vulgaris L.* is a rich source of polyphenols, flavonoids, and tannins, which have potent metal-reducing and free radical scavenging properties. Because of these bioactive components, the plant is especially well suited for green synthesis techniques, where plant-derived metabolites serve as both stabilizing and reducing agents and previously validated in green nanoparticle synthesis and antioxidant-related biomedical applications.

This study hypothesized that green synthesized AuNPs-NAC may enhance ocular permeation and sustained antioxidant delivery, slow or prevent cataractogenesis, and provide a non-surgical, safe, and cost-effective pharmacological method for cataract management. To the best of our knowledge, the evaluation of *Alchemilla vulgaris L.* as a source for AuNP synthesis for anti-cataract applications is reported for the first time. The phytochemical characterization of *Alchemilla vulgaris L.* extracts are presented to clarify its antioxidant, as well as to identify some novel possible biological effects of the plant.

Experimental

Material

Gold (III) chloride trihydrate ($HAuCl_4 \cdot 3H_2O$, ≥99.9% trace metals basis) was obtained from Solarbio (China). N-acetylcarnosine (NAC, ≥98%) was purchased from Solarbio (Beijing, China). Mucin from porcine stomach (Type II, ≥99%) was also supplied by Solarbio (Beijing, China). Phosphate buffered saline (PBS, analytical grade) was purchased from Chemical Point (United Kingdom). 2-2 Diphenyl-1-picrylhydrazyl (DPPH, ≥99%) and L-ascorbic acid (≥99%) were obtained from Sigma-Aldrich (St. Louis, MO, USA). The MTT reagent (3-(4,5-dimethylthiazol-2-yl)-2,5-diphenyltetrazolium bromide, ≥98%) was purchased from Sigma-Aldrich (USA). Fresh aerial parts of *Alchemilla vulgaris L.* (Lady's mantle) were collected, shade-dried, and powdered prior to extraction. Human cataractous lens samples were collected from patients undergoing surgical intervention at Ibn Al-Haitham Teaching Eye Hospital (Baghdad, Iraq) after obtaining written informed consent from all donors in accordance with the Declaration of Helsinki. All reagents were of analytical grade, and deionized water was used throughout the study.

Methods

All experimental protocols were discussed by a scientific committee in the Chemistry Department at Mustansiriyah University, which was formally established according to *PG No.1520 in 10/11/2024* and then the protocols were formally approved by the College of Science at Mustansiriyah University according to *PG No.193 in 17/2/2025.* The study on cataracts was performed in accordance with appropriate guidelines of the Iraqi Ministry of Health.

Plant material identification and collection

We have got a permission from the Department of Biology-Plant branch, College of Science, Mustansiriyah University to collect *the plant material.* The plant was collected with permission from a local authority, which was obtained from Himachal, Pradesh (30-22‹12-33° N; 75-47‹04-79° E), and no plants that were protected or endangered were used. The plant was deposited in the MUST-HERBARIUM in the Mustansiryah University in Baghdad, with a voucher specimen no. MUST#302. The scientific name of the plant *is Alchemilla vulgaris L.*, the family name is Rosaceae, the common name is Lady's Mantle. A qualified botanist in the Department of Biology (Dr. Hadeel Radawi H. Al-Newani), College of Science, Mustansiriyah University, formally identified the plant material. The using of the plant in this study was conducted in accordance with institutional, national, and international regulations, including the IUCN Policy Statement on Research Involving Species at Risk of Extinction and the Convention on International Trade in Endangered Species of Wild Fauna and Flora (CITES).

Preparation of Alchemilla vulgaris L .extract

A measured quantity of *Alchemilla vulgaris L.* (Lady's Mantle) was thoroughly washed several times with distilled water and then air-dried at room temperature. The dried plant was finely ground into a homogeneous powder. Powdered sample (15 g) was mixed with 200 mL of distilled water and heated at 80 °C for 30 minutes under continuous stirring to facilitate extraction. The resulting mixture was filtered through Whatman filter paper, followed by

centrifugation for 10 minutes to obtain a clear, impurity-free supernatant. The filtrate was then stored under refrigerated conditions for subsequent experimental use (36).

Green Synthesis of Gold Nanoparticles (AuNPs)

A volume of 100 mL aliquot of 0.02 M chloroauric acid ($HAuCl_4$) solution was prepared, and the plant extract was dropped wise under ultrasonic agitation at room temperature, for a final ratio of 1:2 (v/v). The color of the mixture gradually changed from pale yellow to reddish-brown, confirming the reduction of Au^{3+} ions and the successful formation of AuNPs. The resulting colloidal suspension was centrifuged at 10,000 rpm for 15 minutes to separate the nanoparticles from the supernatant. The obtained pellet was thoroughly washed several times with distilled water to remove unbound phytoconstituents and residual impurities .To create a stable dry powder, the purified AuNPs and NAC-loaded AuNPs were dried for 24 hours at 40 °C in a lab oven. In order to minimize possible changes in surface functionalization and maintain the structural integrity of the bioactive compounds, this comparatively low drying temperature was chosen. The powders were dried, then allowed to cool to room temperature before being kept in airtight, light-protected containers and stored at 4 °C for subsequent characterization and use (37).

Preparation of AuNPs at Different Concentrations (1–7% w/v)

Three different concentrations of AuNPs (1%, 4%, and 7% w/v) were prepared by dispersing the dried nanoparticles in 10 mL of distilled water to evaluate the effect of concentration on subsequent experimental applications. The prepared suspensions were stored under refrigerated conditions for future use.

Characterization

1. UV–Visible Spectroscopy

UV–Vis absorption spectra were recorded using a Shimadzu UV-1800 spectrophotometer (Shimadzu, Japan) over the wavelength range of 200–800 nm. Samples were diluted 1:10 with distilled water prior to analysis. It was utilized in the characterization of electronic transitions in N-acetylcarnosine (NAC), both $\pi \rightarrow \pi^*$ and $n \rightarrow \pi^*$ transitions of the chromophoric structure of NAC, and to verify the formation of gold nanoparticles (AuNPs), the dispersion, and stability of the gold nanoparticles by observing their typical surface plasmon resonance (SPR) band. All measurements were carried out with a calibrated UV-Vis spectrophotometer under standard conditions to ensure spectral accuracy and reproducibility.(38) .

2. HPLC of the extract

The profiling of the major phenolic and flavonoid constituents of the *Alchemilla vulgaris L.* extract was done with high-performance liquid chromatography (HPLC). The analysis was performed on a SYKAM HPLC system (Germany) equipped with a C18-ODS column (25 cm x 4.6 mm). The mobile phase consisted of methanol:deionized

water:formic acid (70:25:5, v/v/v), with a flow rate of 1.0 mL/min, and was detected at 280 nm using a UV detector. The injection volume was 0.1 mL. Identification of the compounds was performed by comparing their retention times (Rt) with those of authentic reference standards chromatographed under the same conditions. Chloroform maceration, ultrasonic treatment, and butanol partitioning were used to obtain a purified, dry extract suitable for chromatographic analysis. This was a way to provide reliable, reproducible, and selective profiling of the bioactive phytochemical molecules in the extract.(39).

3. Fourier Transform Infrared Spectroscopy (FTIR)

FTIR spectra were recorded using a Bruker FTIR spectrometer (Bruker, Germany) to determine the functional groups and spectral properties of N-acetylcarnosine (NAC) and the *Alchemilla vulgaris L.* (*Lady's* Mantle) extract. The dried AuNPs and NAC-loaded AuNPs were analyzed directly using the attenuated total reflectance (ATR) mode without additional sample preparation ,The spectra were taken in the mid-infrared (650-4000 cm-1) range to determine characteristic stretching and bending vibrations of the hydroxyl (O-H), amine (N-H), carbonyl (C=O), and C-N functional groups. The FTIR analysis was used to obtain information on the chemical composition of NAC and the biomolecules in plants, and to determine their functions in nanoparticle reduction and stabilization. A calibrated FTIR spectrometer was used to measure all samples under controlled conditions to ensure the accuracy and reproducibility of the spectra.(40).

4. X-ray Diffraction (XRD)

The crystalline structure of the synthesized AuNPs and NAC-loaded AuNPs was analyzed using a Philips PW1730 X-ray diffractometer (Philips, Netherlands) equipped with Cu-Kα radiation (λ = 1.5406 Å). Diffraction patterns were recorded over a 2θ range of 20°–80° at a scanning rate of 0.02° per second under standard operating conditions. The obtained diffraction peaks were compared with standard reference data (JCPDS database) to confirm the face-centered cubic (fcc) structure of gold nanoparticles (41). XRD was also used to confirm the nanoparticles' crystallinity and determine the mean crystallite size. All the diffraction patterns were measured with a calibrated XRD diffractometer under standard instrumental conditions, ensuring accuracy and reproducibility(42)

5. Field Emission Scanning Electron Microscopy (FESEM)

The morphology and surface properties of the synthesized AuNPs and NAC-loaded AuNPs were investigated by field emission scanning electron microscopy (FESEM) analysis using a TESCAN MIRA3 microscope (TESCAN, Czech Republic). Double-sided conductive carbon tape was used to mount dried nanoparticle samples on aluminum stubs, and a thin layer of gold was sputter-coated to improve conductivity. To assess the shape and size distribution of the particles, micrographs were taken at a 15 kV accelerating voltage and at the proper magnifications.(43)

6. Atomic Force Microscopy (AFM)

The nanoscale surface topography and morphology of the prepared materials were determined using NTEGRA Aura Atomic Force Microscope (NT-MDT Spectrum Instruments, Russia) to look at the surface topography and particle morphology in more detail. Clean glass slides were used to hold dried nanoparticle samples, which were then left to air-dry before being imaged. Measurements were conducted in semi-contact mode under ambient conditions to acquire high-resolution surface morphology and particle size data.(43)

7. Zeta Potential Measurement

The surface charge properties and colloidal stability of the developed nanoparticle formulations were determined by measuring zeta potential. The data were analyzed using HORIBA SZ-100 Zeta Potential Analyzer (HORIBA Ltd., Japan), which is based on electrophoretic light scattering (ELS) to measure the electrophoretic mobility and zeta potential of individual particles. Experiments were conducted at 25 °C after appropriate dilution of the nanoparticle suspension in distilled water to avoid multiple scattering effects. Each measurement was conducted in triplicate to provide a clear evaluation of interparticle electrostatic interactions, dispersion behavior, and the impact of surface functionalization on nanoparticle stability. (44).

In-vitro Antioxidant Activity (DPPH Assay)

To assess the antioxidant activity of AuNPs and AuNPs loaded with NAC, 2,2-diphenyl-1-picrylhydrazyl (DPPH) scavenging assay was used. This technique is based on the reduction of the stable DPPH radical, which causes a decrease in absorbance at 517 nm which is proportional to the tested samples' ability to scavenge radicals. DPPH stock solution was prepared by dissolving 4 mg DPPH in 3 mL of analytical-grade methanol, and kept in the dark until it was needed. A volume of 250 µL of DPPH solution was combined with 250 µL of different concentrations of the tested sample, which was then allowed to sit at room temperature for 30 minutes in the dark. AuNPs (1%, 4%, and 7% w/v), NAC (0.05, 0.1, and 0.3 mM loaded with 7% w/v AuNPs) were tested against ascorbic acid (10 to 100 mg/mL) as a positive control. A UV-Visible spectrophotometer was used to measure absorbance at 517 nm, using methanol as the blank. For comparison, DPPH and methanol without sample were used as a control (45). All measurements were performed in triplicate (n = 3) and expressed as mean ± standard deviation (SD). The antioxidant activity of the samples was evaluated using the DPPH free radical scavenging assay, and the percentage of inhibition was calculated according to the following equation:

$$100 * \frac{A\infty - Ac}{Ac} = \% I$$

Where $A\infty$ represents the absorbance of the sample and Ac represents the absorbance of the control

Cytotoxicity Assay (MTT)

The cytotoxicity of AuNPs, Alchemilla vulgaris L. extract, and AuNPs–NAC formulations was evaluated using the MTT assay on human lens epithelial cells (HLE-B3; ATCC® CRL-11421™) to see how toxic AuNPs, Alchemilla vulgaris L. extract, and AuNPs–NAC formulations were. Under standard incubation conditions (37 °C, 5% CO_2, humidified atmosphere), cells were grown in Eagle's Minimum Essential Medium (EMEM) with 20% foetal bovine serum (FBS) and 1% penicillin-streptomycin (100 U/mL penicillin and 0.1 mg/mL streptomycin). Cells were placed in 96-well plates and given 24 hours to attach before being treated. After that, cells were exposed to the test formulations at different concentrations (25, 50, 100, 200, and 400 µg/mL) for 24 hours. After treatment, each well received 20 µL of MTT solution (5 mg/mL) and was left to sit for 4 hours to let formazan crystals form. We carefully took off the supernatant and dissolved the formazan crystals in dimethyl sulfoxide (DMSO). A microplate reader was used to measure absorbance at 570 nm. Cell viability (%) was calculated relative to untreated control cells. All experiments were performed in triplicate ($n = 3$) and expressed as mean ± standard deviation (SD). Statistical analysis was carried out using one-way ANOVA followed by Dunnett's multiple comparisons test, with $p < 0.05$ considered statistically significant. IC_{50} values were determined using nonlinear regression analysis of concentration–response curves.(45).

Drug Release Study

The release kinetics of NAC from AuNPs formulations were evaluated using a dialysis bag diffusion technique. Dialysis membranes with a molecular weight cut-off (MWCO) of 7–14 kDa were employed, each containing 1 mL of the nanoparticle suspension. Three dialysis bags were immersed separately in 50 mL of phosphate-buffered saline (PBS) containing mucin derived from porcine stomach to simulate the ocular environment. The experiments were performed at room temperature under gentle stirring at different pH values (6.0, 7.4, and 8.0) to mimic physiological and pathological ocular conditions. Aliquots were withdrawn at predetermined time intervals ranging from 0.25 to 24 hours, and the concentration of released NAC was quantified spectrophotometrically at 220 nm using a UV–Vis spectrophotometer(46, 47).

Ex-vivo Lens Transparency Evaluation

Human cataractous lens samples obtained from patients with diabetic or renal-failure–associated cataracts were immersed in solutions containing AuNPs, 7% w/v loaded with varying concentrations of NAC ranging from 0.01 to 0.3 mM. The lenses were incubated for up to 15 days, during which progressive optical changes were monitored using digital imaging. A gradual improvement in lens optical clarity was observed, particularly in samples treated with NAC concentrations between 0.1 and 0.3 mM. This enhancement in clarity indicates improved permeability of the antioxidant molecules through the lens capsule and suggests that NAC-loaded AuNPs effectively protect lens proteins from oxidative modification and structural degradation (46-48), see equation (1).

Loading of NAC onto AuNPs

For the loading NAC onto AuNPs at concentrations of 1%, 4% and 7% (w/v), precisely 0.268 g of NAC was weighed and added to each AuNPs suspension. The mixtures were gently stirred and allowed to incubate at room temperature for 24 hours to ensure optimal adsorption of NAC molecules onto the nanoparticle surfaces. Following incubation, the suspensions were centrifuged to separate the unbound NAC, and the supernatants were collected for analysis. The encapsulation efficiency (EE %) and drug-loading capacity (DL %) of NAC were subsequently calculated to evaluate the loading performance. The supernatant was analyzed at 220 nm (UV–Vis) to determine the unbound drug concentration. Encapsulation efficiency (EE %)(49) and drug loading (DL %)(50) were calculated as equation 1 and 2:

$$\% EE = \frac{total\ drug\ added - free\ (unencapsulated\ )drug}{Total\ drug\ added} * 100 \quad \ldots\ldots\ldots (1)$$

$$\% Drug\ loading = \frac{\text{amount of drug loaded into NPs}}{\text{Total weight of dried NPs}} * 100 \quad \ldots. (2)$$

Calibration Curve for NAC

The calibration curve was constructed to accurately quantify NAC concentrations during the drug loading and encapsulation studies. A series of standard NAC solutions (0.005–0.3 mM) were freshly prepared, and their absorbance values were measured at 220 nm using a UV–Vis spectrophotometer under optimized analytical conditions. The resulting calibration plot demonstrated strong linear correlation (R^2 = 0.989), confirming strict compliance with Beer–Lambert's law, and the regression equation was subsequently utilized to calculate the concentration of unbound NAC and to precisely determine both the drug loading and encapsulation efficiencies in the nanoparticle formulations(51) .

In Silico and Computational Analysis

The computational study was conducted to elucidate the molecular pattern and interaction behavior of NAC. Pharmacophore modeling was performed using Pharmit to identify the spatial distribution of the functional groups responsible for protein binding. The analysis revealed distinct hydrophobic regions, hydrogen bond–forming domains, and an anionic (carboxylic) area, indicating the molecule's potential to establish electrostatic and polar interactions with various proteins(52). Pharmacokinetic and toxicity properties were further evaluated using SwissADME and ProTox-II platforms. The results demonstrated that NAC possesses excellent drug-like characteristics and an almost negligible toxicity profile, with an estimated LD_{50} of 14,930 mg/kg, and exhibits high gastrointestinal absorption while lacking blood–brain barrier permeability — confirming its safety for ophthalmic therapeutic applications(53, 54).

Molecular docking simulations were carried out using AutoDock 1.2.3 to explore the interactions between NAC and lens proteins. The results revealed strong binding affinities ranging from −5.4 to −6.0 kcal/mol, with multiple hydrogen

bonds formed with the amino acid residues Tyr45, Arg79, and Asp17. These interactions suggest that NAC contributes to the stabilization of lens proteins and prevents their abnormal aggregation, thereby preserving lens transparency. These computational findings are in strong agreement with the experimentally observed antioxidant and anti-cataract properties of NAC(55).

Statistical analysis

All *in vitro* experiments were in triplicate (n = 3), and the data are expressed as mean ± standard deviation (SD). Statistical analyses were performed using IBM SPSS Statistics software, version 29 (IBM Corp., Chicago, IL, USA), and GraphPad Prism, version 8.4.3 (GraphPad Software, San Diego, CA, USA). One-way analysis of variance (ANOVA) followed by Dunnett's multiple comparisons test were used to compare groups statistically. This statistical approach was applied to both DPPH radical scavenging and MTT cytotoxicity assays. The alpha level was 0.05. Using a four-parameter logistic (4PL) model with a variable slope, nonlinear regression analysis was used to make dose–response curves. The 4PL model was specifically used for the calculation of IC_{50} values derived from concentration–response curves. We used the profile likelihood method to find the 95% confidence intervals (CI) for the IC50 values. The coefficient of determination (R^2) was used to check how well the model fit the data. A p-value of less than 0.05 was considered a statistically acceptable.

Safety considerations

All of the experiments were done following standard safety rules for labs. Lab coats, gloves, and safety glasses, were used during experimental parts. Standard laboratory protocols were utilized to handle chemical reagents and nanomaterials so that we reduced the risk of exposure. Humans' samples were handled, stored, and properly disposed, in accordance with Mustansiriyah University and Ministry of Health biosafety and ethical protocols.

Limitations of the study

There are some limitations to the current study. The *ex vivo* human lens model, while highly relevant for assessing lens transparency, does not fully replicate the complex physiological conditions of the living eye. Extended incubation times and physiologically appropriate pH levels were used to overcome this restriction. Handling, storage, and processing procedures were challenging to maintain lens integrity because the availability and handling of human cataractous lenses were restricted, and tissue sensitivity to mechanical and biochemical damage. Standardized extraction and regulated synthesis conditions reduced the potential impact of *Alchemilla vulgaris L* phytochemical composition variability on the AuNPs synthesis reproducibility. Lastly, full clinical application still requires *in vivo* validation, which was outside the purview of this study.

Results and discussion

Synthesis and Characterization

AuNPs were synthesized through an environmentally friendly (green) approach using *Alchemilla vulgaris L*. (lady's mantle) extract as a natural reducing and capping agent. The extract facilitated the reduction of chloroauric acid ($HAuCl_4$) to elemental gold, as evidenced by a distinct color change from pale yellow to reddish brown—a classical visual indication of surface Plasmon resonance (SPR)(37, 56). The formation of AuNPs was further confirmed by UV–Vis spectrophotometry, which exhibited a characteristic absorption peak at 520 nm corresponding to the SPR band of spherical gold nanoparticles(57) as shown in Figure (1A), Additionally, NAC exhibited a maximum at 220 nm, which is attributed to its characteristic electronic transitions — specifically the $n \rightarrow \pi$ and $\pi \rightarrow \pi$ transitions within its functional chromophoric groups, which is considered a characteristic fingerprint of NAC and was employed for quantitative determination using HPLC and UV–Vis spectroscopic analyses (58). The absorption band at 220 nm provided an analytical identification of of NAC in complex nanoconjugated systems(59), distinguishable from the surface Plasmon resonance (SPR) signal of AuNPs, as shown in Figure (1B).

Fourier-transform infrared (FTIR)

The Fourier-transform infrared (FTIR) spectrum of the *Alchemilla vulgaris L.* extract revealed characteristic vibrational peaks confirming the presence of phenolic compounds, flavonoids, and carboxylic groups—key phytoconstituents responsible for the bioreduction of gold ions to elemental gold. The broad absorption band corresponding to N–H and O–H stretching vibrations, typically associated with phenols, alcohols, and proteinaceous compounds, indicated their crucial involvement in the reduction process through electron donation. The prominent C=O stretching observed in the region characteristic of carboxylic acids and esters further suggests the presence of flavonoids and organic acids within the extract(40). In addition, bands at approximately 1610 cm^{-1} and 1213 cm^{-1} correspond to C=C and C–O stretching vibrations, respectively, confirmed the polyphenolic nature of the extract. The absorption peaks below 1000 cm^{-1} were attributed to bending vibrations of C–H and metal–oxygen (M–O) bonds, which may represent potential binding sites for gold ions, facilitate the nucleation and stabilization of AuNPs complexes. These findings collectively substantiate the pivotal role of *Alchemilla vulgaris L.* extract as a reducing and capping agent in the green synthesis of AuNPs (60). Table 1S and Figure 1 (C and D) summarizes the characteristic stretching vibration frequencies corresponding to the functional groups.

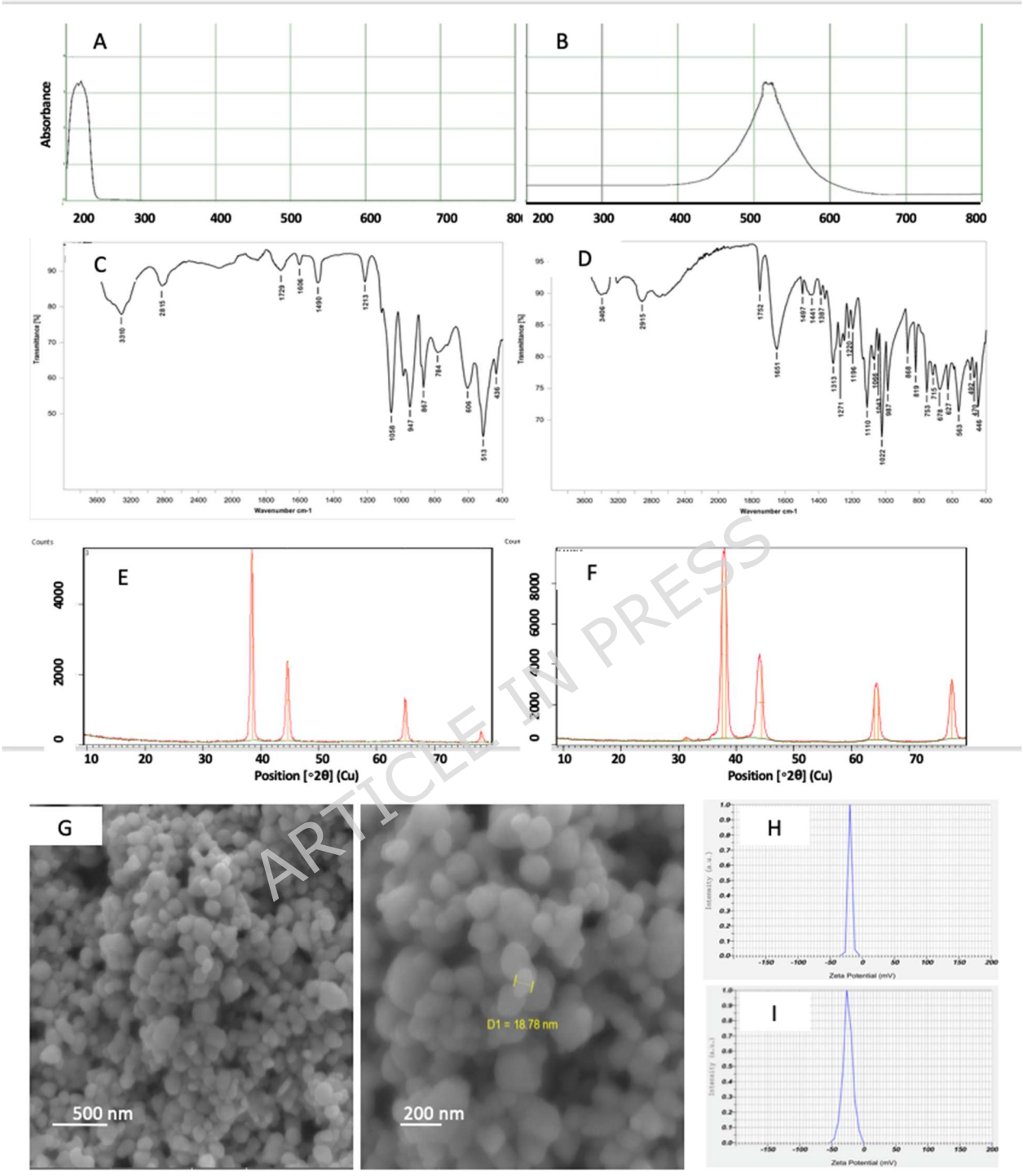

Figure 1. Characterization results of the AuNPs before and after loading with NAC. A) UV–Vis spectra of AuNPs and B) for NAC, C) FTIR spectra of AuNPs, D) FTIR spectra of AuNPs-NAC, E), XRD patterns of AuNPs, F) XRD of AuNPs-NAc, G) FESEM images of AuNPs in 500 nm and 200 nm scale bars, H) ζ of AuNPs and I) ζ of AuNPs-NAC.

The FTIR spectrum of NAC exhibited well-defined absorption bands characteristic of its functional groups, confirmed the molecular integrity of the compound. A broad and intense band observed around 3406 cm^{-1} corresponded to the overlapping N–H and O–H stretching vibrations, indicative of imidazole and amide functionalities. The absorption peak at 2915 cm^{-1} was attributed to aliphatic C–H stretching, while the sharp band at 1762 cm^{-1} represented the carbonyl (C=O) stretching vibration associated with the acetyl moiety of NAC(61).

Additionally, distinct peaks at 1651 cm^{-1} and 1497 cm^{-1} correspond to amide I and amide II vibrations, respectively, confirmed the presence of peptide linkages within the molecular backbone. The strong absorptions in the region of 1000–1200 cm^{-1} assigned to C–N and C–O stretching vibrations, reflecting the existence of carboxyl and amide groups. The low-frequency bands appeared between 524 and 450 cm^{-1} related to skeletal carbon vibrations, further validating the structural framework of the NAC molecule (51, 61).

Overall, these spectral findings corroborate the characteristic vibrational profile of NAC and provide a definitive spectroscopic signature for its identification and subsequent interaction with AuNPs in the synthesized nanoconjugated system. Table 1 and Figure (1) summarize the characteristic stretching vibration frequencies corresponding to the functional groups

X-ray diffraction (XRD)

The X-ray diffraction (XRD) pattern of AuNPs in Figure 2 (C) displayed four prominent Bragg reflections at $2\theta \approx$ 38.21°, 44.4°, 64.6°, and 77.5°, which are indexed to the (111), (200), (220), and (311) planes of face-centered cubic (FCC) Au and match the standard reference pattern (JCPDS 04-0784). Notably, the (111) reflection exhibited the highest intensity (≈8172 counts), indicating a preferred orientation along (111)—a behavior frequently reported for stable AuNPs produced by plant-mediated (green) routes. The corresponding interplanar spacings (d) are consistent with FCC Au (e.g., ~2.35 Å for (111), ~2.04 Å for (200), ~1.44 Å for (220), ~1.23 Å for (311)), further confirming phase purity and crystallinity (62).

Crystallite sizes estimated from the Scherrer equation ($D = K\lambda/\beta cos\theta$)(63) fell in the 20–35 nm range, in agreement with SEM/AFM observations; the sharp peaks and narrow full width at half maximum (FWHM ≈ 0.23–0.46) reflect high crystallinity and low lattice strain. The absence of spurious reflections evidences complete reduction of Au^{3+} to metallic Au and a high-purity product(64). Together with FTIR data, these results support the dual role of plant polyphenols as reducing and capping agents, which is well-documented in green syntheses of noble-metal nanoparticles, as shown in Figure 1 (E). XRD pattern obtained after loading AuNPs with N- NAC (Figure 2 D) revealed that the principal reflections characteristic of face-centered cubic (FCC) gold was preserved at 2θ values of 38.5°, 44.6°, 64.9°, and 78.09°, corresponding to the (111), (200), (220), and (311) planes, respectively. This confirms that the intrinsic crystalline structure of metallic gold remained intact after functionalization(65). A slight shift of the (111) peak from 38.21° to 38.5°, accompanied by a small decrease in relative intensity from 100 % to 98.3 %, suggests a minor degree of lattice strain and surface modification induced by the adsorption of NAC molecules onto the nanoparticle surface(66), Figure 1 (F).

FESEM test

High-resolution field emission scanning electron microscopy (FESEM) images (Figure 1 G) revealed that the green-synthesized AuNPs exhibited predominantly spherical to quasi-spherical morphologies with a uniform size distribution and minimal aggregation(67). The average particle diameter ranged between 15 and 30 nm, which closely corresponds to the crystallite size estimated from XRD analysis using the Scherrer equation. Previous studies have consistently reported that the spherical morphology of green-synthesized AuNPs arises from the polyphenolic-mediated reduction mechanism(68), wherein plant-derived phytoconstituents act simultaneously as reducing and capping agents. These bioactive compounds donate electrons to reduce Au^{3+} ions to metallic Au^{0} while stabilizing the nanoparticle surface, thereby preventing agglomeration and enhancing colloidal stability(69). Such biomolecule-assisted synthesis routes are widely recognized for producing well-defined, stable nanostructures suitable for biomedical and therapeutic applications. At higher magnifications (135–700 K×), FESEM images revealed well-defined clusters of nanostructures composed of smooth-surfaced, discrete particles with delineated boundaries, indicating high crystallinity and homogeneous nucleation during the synthesis process. The narrow inter particle spacing further reflects the strong stabilizing efficiency of the *Alchemilla vulgaris L* extract, which effectively prevents coalescence and preserves nanoscale dispersion (37, 57, 70). At lower magnifications (1–10 µm), the FESEM images exhibited a continuous granular texture in which the nanoparticles appeared interconnected, forming dense network-like architectures. This phenomenon can be attributed to solvent evaporation during drying, which induced the assembly of individual nanocrystals into cohesive aggregates—a commonly reported feature in metallic nanostructures synthesized through green, phytochemical-mediated methods (57, 71)

Zeta potential (ζ) test

Zeta potential **(ζ)** analysis showed that the green-synthesized gold nanoparticles exhibited a surface potential of −25 mV, accompanied by an electrophoretic mobility of 1.93×10^{-4} $cm^2 \cdot V^{-1} \cdot s^{-1}$ at 25°C, consistent with values commonly reported for phytochemically stabilized AuNPs colloids (72). The measurement was conducted in a medium of viscosity 0.985 mPa·s and conductivity 0.090 $mS \cdot cm^{-1}$, indicating a dispersed colloidal system controlled by electrostatic repulsion between nanoparticles. According to established colloidal stability criteria, **(ζ)** values ≥ |30| mV indicate stable dispersions, whereas values between |20–30| mV correspond to systems with moderate yet functionally sufficient stability—which aligns with the measured value (73). The negative surface charge was attributed to deprotonation of carboxyl and phenolic groups in the plant extract, which acts simultaneously as a reducing and capping agent during nanoparticle formation(74). Previous studies reported that the ζ of green-synthesized AuNPs typically ranged from −15 to −50 mV, confirmed that the obtained value lies within the expected and acceptable stability range for phytochemical-mediated nanogold (75).

Following the loading of AuNPs with NAC, the dispersion exhibited an electrophoretic mobility of 1.001×10^{-4} $cm^2 \cdot V^{-1} \cdot s^{-1}$ and a viscosity of 0.894 mPa·s at 25°C under an applied electric field of 3.4 V. The ζ measurement revealed a decrease from −25 mV to −18 mV, which can be attributed to the increase in the thickness of the organic corona surrounding the nanoparticle surface(76), as well as the surface coverage by NAC molecules. The functional

groups of NAC — including carboxyl, imidazole, and amide moieties — interact with the negatively charged sites originally present on the nanoparticles, resulting in partial masking of surface charge and subsequent reduction in the overall negative ζ potential (77, 78), see Figure (1H and I).

AFM for AuNPs / AuNPs-NAC

Atomic force microscopy (AFM) analysis (scan areas of 0.50 × 0.50 µm and 0.20 × 0.20 µm) revealed a compact layered arrangement of the AuNPs, Figure 2 (A and B) The surface topography exhibited height parameters ranging between Sa = 1.17–7.02 nm and Sq = 1.49–9.74 nm, indicated a surface of moderate nanoscale roughness(79). The surface bearing characteristics derived from the Firestone–Abbott (material ratio) curve demonstrated a valley fraction, the presence of nanoscale depressions distributed across the surface(80).The surface area ratio (Sdr) reached 42.42%, referred to developed surface area, which is favorable for surface adsorption and molecular anchoring. The autocorrelation length (Sal ≈ 62 nm) suggested that the lateral

spacing between surface features falls within the nanometric regime, consistent with the expected spatial distribution

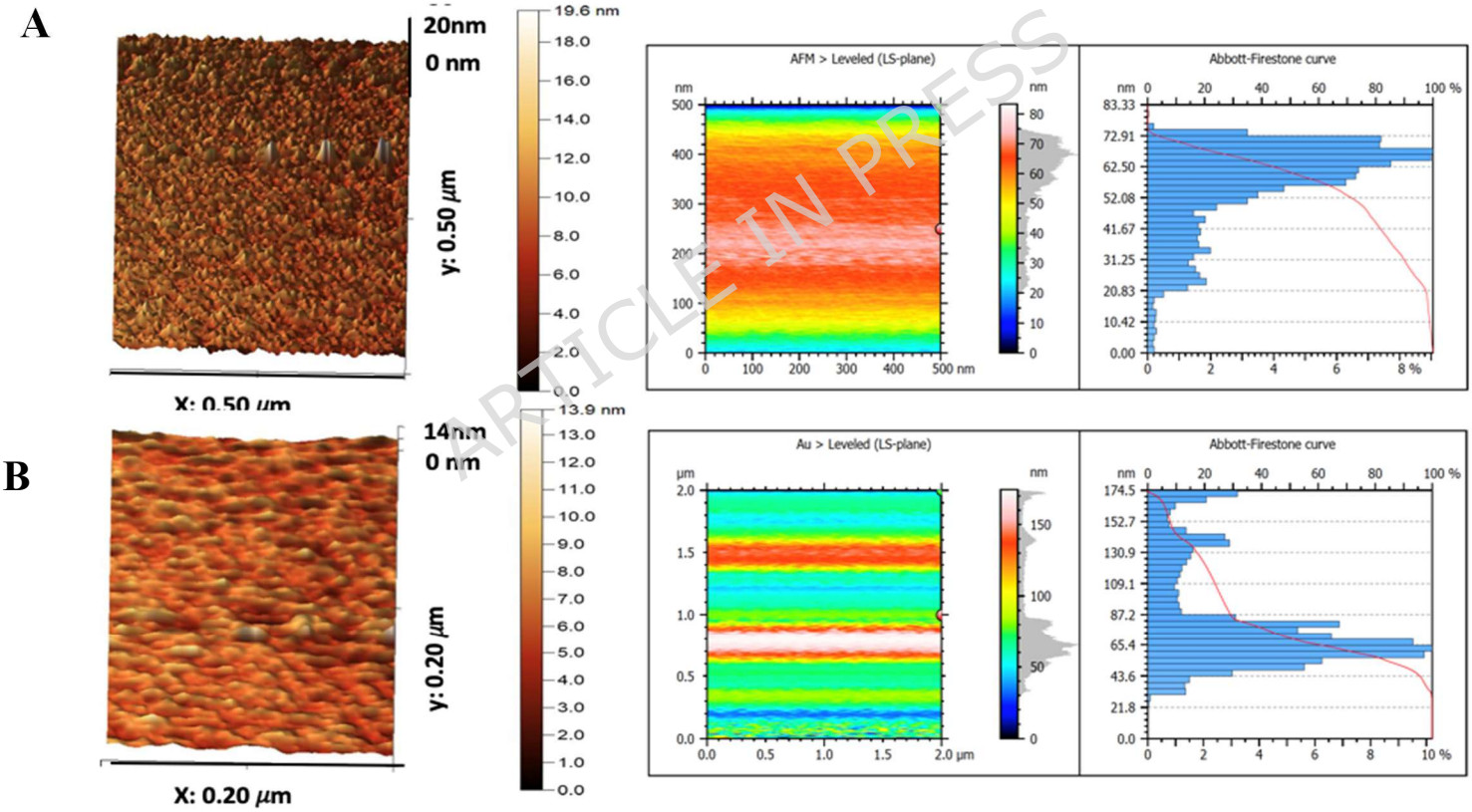

of AuNPs (81).

Figure 2. AFM imaging for Au NPs before loading (A) and after loading (B)

After loading AuNPs with NAC, the sample topography scanned 2.0 × 2.0 µm, which revealed an alteration in the nanosurface architecture. The surface roughness parameters (Sa) increased from 1.17–7.02 nm to 21.44 nm and Sq

increased from 1.49–9.74 nm to 25.83 nm, indicated formation of a continuous organic NAC coating layer on the nanoparticle surface. Such increases in height-based roughness parameters are associated with molecular adsorption and corona formation on nanostructured surfaces(82). Furthermore, the Firestone–Abbott bearing ratio analysis demonstrated a surface transition characterized by higher peak prominence (S-pk) and reduced valley depth (S-vk) compared to the unmodified nanoparticles. The increase in S-pk indicated rise of nanoscale protrusions caused by NAC anchoring on surface-active sites, while the decrease in S-vk indicated filling and smoothing of nanoscale depressions, confirming successful surface loading and molecular occupancy(83). The surface complexity ratio (Sdr) exhibited an increase following NAC conjugation, due to developed surface area raised from the organic molecular layer overlaying the native nanoparticle topography. Additionally, the autocorrelation length (Sal) increased from ≈ 62 nm (pre-loading) to ≈ 116 nm after NAC coating, indicated a transition from localized roughness to more laterally continuous surface morphology. This behavior is consistent with the formation of a uniform, coherent molecular layer that bridges peaks and valleys across the nanosurface.(82).

High-performance liquid chromatography (HPLC) analysis of Alchemilla vulgaris L. extract

High-performance liquid chromatography (HPLC) for *Alchemilla vulgaris L.* extract was performed using a C18-ODS column (25 × 4.6 mm) with chromatographic conditions, which are recognized as optimal for the separation of phenolic and flavonoid compounds(39). Among the identified phytoconstituents, rutin and quercetin are of particular relevance due to their well-established antioxidant and anti-glycation activities. Rutin has been demonstrated to significantly suppress advanced glycation end-product (AGE) formation and attenuate oxidative protein modification, thereby limiting structural destabilization of long-lived proteins(1, 2). Given that AGE accumulation promotes crystallin cross-linking and aggregation during cataractogenesis, thus, inhibition of glyco-oxidative pathways represents a mechanistically relevant anti-cataract strategy(3). Quercetin likewise exhibits potent free-radical scavenging capacity and has shown protective effects in human lens epithelial cells by mitigating oxidative stress-induced apoptosis(4). Phytochemical profile also confirms the presence of polyphenols in Alchemilla vulgaris, accounting for its intrinsic redox activity(5). Importantly, flavonoids such as rutin and quercetin can function as reducing and stabilizing agents during plant-mediated green synthesis of AuNPs, facilitating Au(III) reduction and surface capping through electron-donating hydroxyl groups, thereby conferring simultaneous therapeutic and nanotechnological relevance(6).

Detection at 280 nm is also well-established for flavonoid and phenolic compound identification due to their strong aromatic conjugation and UV absorbance characteristics(84). The retention time (Rt) and peak matching results demonstrated clear correspondence between sample constituents and their respective standards. The rutin peak appeared at Rt = 2.26 min, matching the standard value, and accounted for 16% of the total peak area. Quercetin was identified at Rt = 3.77 min (standard Rt = 3.79 min) with a relative area of 11%. Ferulic acid showed a characteristic peak at Rt = 5.95 min, closely matching its standard (Rt = 5.98 min), contributing ~11% of the signal. Kaempferol was detected at Rt = 9.91 min (standard Rt = 9.90), while chlorogenic acid was observed at Rt = 11.87 min, also

consistent with the reference value (Rt = 11.80 min). A flavonoid peak at Rt = 4.11 min represented approximately 15% of the total signal. Quantitative analysis revealed the following concentrations (ppm) in the extract shown in Table (1) and Figure 1S.

Table 1. Quantitative analysis of the extract content

Compound	Concentration (ppm)
Rutin	188.9
Gallic acid	132.6
Quercetin	74.9
Kaempferol	57.9
Ferulic acid	88.9
Apigenin	90.8
Chlorogenic acid	74.9

These results confirm that the plant extract is rich in phenolic and flavonoid constituents, which are well-known for their potent antioxidant activity, as well as their ability to neutralize and inhibit free radical species, thereby supporting their role in enhancing the bioactivity and functional performance of the synthesized AuNPs (85).

MTT test

Human lens epithelial cells (HLE-B3) were employed as an *in vitro* model to evaluate the cytocompatibility of the plant extract, AuNPs and AuNPs-NAC formulations. The cytotoxicity was assessed using the MTT assay (86). The results demonstrated that cells retained 80–96% viability when treated with the plant extract (0–400 µM), which indicated good biocompatibility. Likewise, the AuNPs-NAC exhibited 73–96% cell viability over the same concentration range, with a gradual decrease in viability observed at higher concentrations. According to the standard ISO 10993-5 cytotoxicity classification, a material is considered non-cytotoxic if cell viability remains ≥70%. All tested samples exceeded this threshold, confirming their low or negligible cytotoxicity within the concentration range.(87, 88). This biocompatible response can be attributed to the antioxidant properties of NAC, which enhances intracellular glutathione (GSH) homeostasis and counteracts oxidative stress. Experimental evidence from lens and retinal cell studies supported that NAC, and structurally related molecules, protect ocular cells against oxidative damage, thereby maintaining cell integrity and metabolic activity(89), consistent with the viability observed in this study. Figure 2S (A-D) shows MTT test for extract and AuNPs loaded with difference concentrations of NAC.

Table 2. Comparative IC_{50} Values of *Alchemilla vulgaris L.* Extract and NAC-Loaded AuNPs in HLE-B3 Cells (MTT Assay)

	Extract	Au- NAC (0.05 µg/mL)	Au-NAC (0.1 µg/mL)	Au-NAC (0.3 µg/mL)
IC_{50}	388.9	354.7	306.2	231.5

DPPH assay

The DPPH assay conducted for the *Alchemilla vulgaris L.* extract (Figure 3S) demonstrated a free-radical scavenging capacity, with inhibition exceeding 90%, which is attributed to its rich content of phenolic and flavonoid compounds(90). In contrast, unloaded AuNPs exhibited a moderate scavenging activity (20–60%), $p < 0.02$, consistent with their surface electron–transfer catalytic role, rather than functioning as direct antioxidant agents(91). The AuNPs-NAC displayed an enhanced radical scavenging effect, with inhibition levels ranging between 72–88%, %), $p < 0.02$, which increased proportionally with NAC concentration. This enhancement is primarily attributed to the thiol-functional groups in NAC, which facilitated reduction of reactive ROS and promoted regeneration of intracellular glutathione (GSH), in addition to strengthening surface interaction and bioactivity through their association with the nanoparticle interface. The AuNPs–NAC therapy system exhibited an antioxidant profile, underscoring its potential to ameliorate oxidative stress associated with lens opacity and cataractogenesis(34). Figure 3S (A) shows DPPH inhibition% for AuNPs and AuNPs - NAC compared to ascorbic acid concentrations.

Drug release

The *in vitro* release profile of NAC using a dialysis membrane showed a biphasic kinetic pattern, characterized by an initial burst release during the first 2–4 hours, followed by a sustained diffusion-controlled release phase extending up to 24 hours. This biphasic behavior is consistent with controlled-release nanocarrier systems, where surface-associated drug is released rapidly, while drug encapsulated within the carrier matrix diffuses more gradually over time(92). Figure 3S (B) showed a pH-dependent release pattern, where the release rate was highest at pH 6, moderate at pH 7.4, and lowest at pH 8. This trend aligns with the known behavior of pH-responsive nanosystems, in which mildly acidic environments weaken drug–carrier interactions, thereby enhancing molecular diffusion and accelerating release (93). Since tear fluid maintains a physiological pH of approximately 7.4–7.6, the release profile at pH 7.4 considered the most physiologically relevant for ocular delivery systems. (94). The NAC-loaded AuNPs also demonstrated an encapsulation efficiency (EE ≈ 86.1%) and an adequate loading capacity (≈ 19.3%), values that fall within the optimal range for ophthalmic nanocarriers, which may highlight s drug retention within the delivery matrix while maintaining colloidal stability. Overall, the Au-NPs-NAC system is designed to deliver a rapid initial therapeutic dose, followed by sustained release under physiological ocular conditions, (95). Figure 3S (B) shows drug release at different pHs.

In Silico Molecular Docking Studies

Molecular docking analysis revealed that the ligand exhibits a high binding affinity and selective interaction toward lens crystallin proteins, which play a critical role in maintaining lens transparency(96). Any disruption in the structural integrity or stability of these crystallins can lead to their unfolding or aggregation, ultimately contributing to the development and progression of lens opacification (cataract)(97).

1- Interaction with αB-Crystallin (PDB: 2WJ7)

Molecular docking results showed that the ligand formed multiple hydrogen bonds with key residues Asp17, Lys19, and Arg57, generating a compact and stable hydrogen-bonding network at the protein-binding interface. The formation of dense hydrogen-bonding networks is known to enhance ligand–protein binding affinity and stabilize the local secondary structure of crystallin proteins(55, 98).As shown in Figure (3)

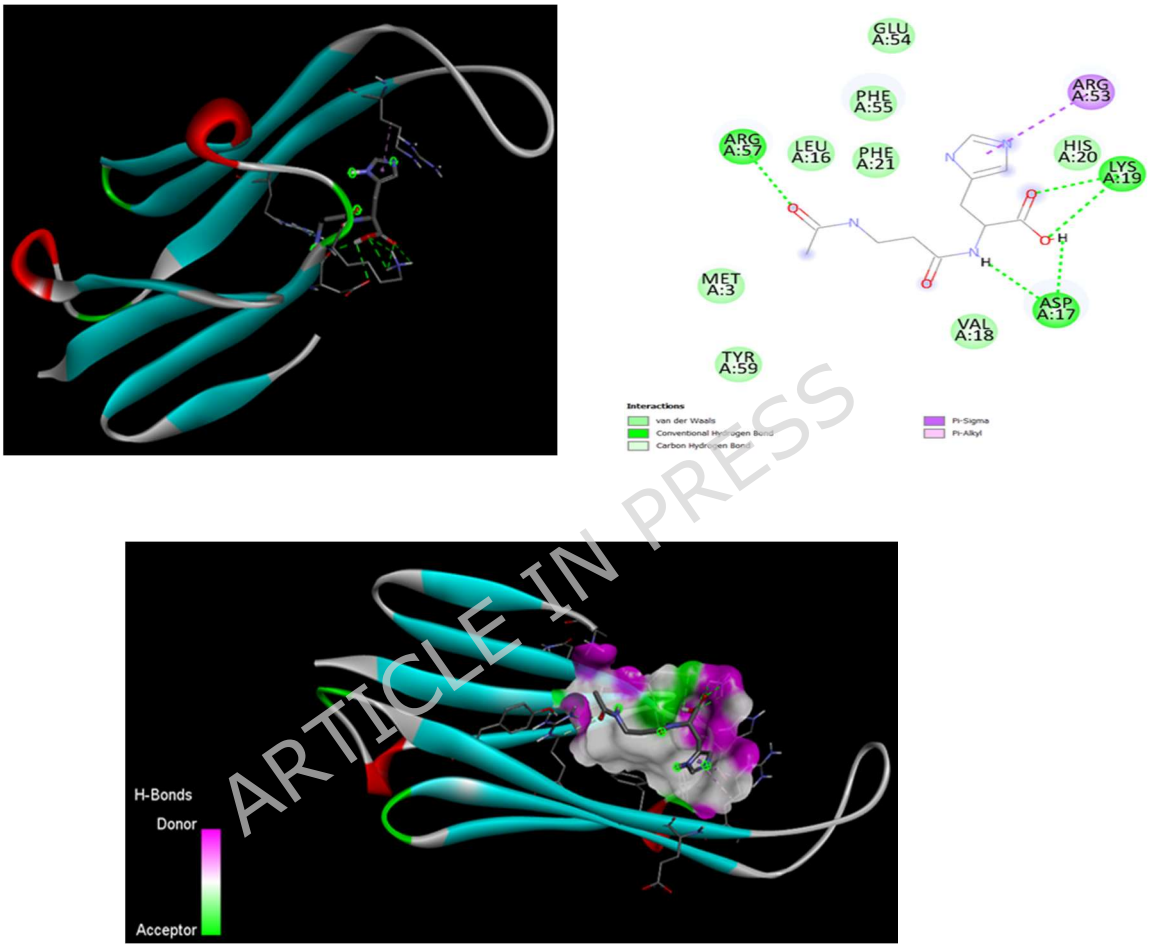

Figure 3. Molecular docking results of the ligand with Human αB Crystallin (PDB ID: 2WJ7): (a) Docking pose of the ligand in the active site, (b) 2D representation of the ligand–protein interactions, and (c) hydrogen bond interaction map.

2. Interaction with βB1-Crystallin (PDB: 1OKI)

The ligand exhibited a stable binding affinity of −5.8 kcal/mol, mediated through hydrogen-bond interactions with the amino acid residues Asp233, Trp236, and Gly98, in addition to forming dual stabilizing interactions with Lys117. These interactions suggest a well-anchored ligand orientation within the binding pocket of βB1-crystallin. βB1-crystallin is a structurally essential lens protein that contributes to oligomer assembly, solubility maintenance, and

refractive index stability in the lens. Disruption of β-crystallin oligomerization has been strongly associated with lens opacification and cataract formation, as aberrant aggregation leads to light-scattering protein complexes within the lens matrix(99) , Figure (4).

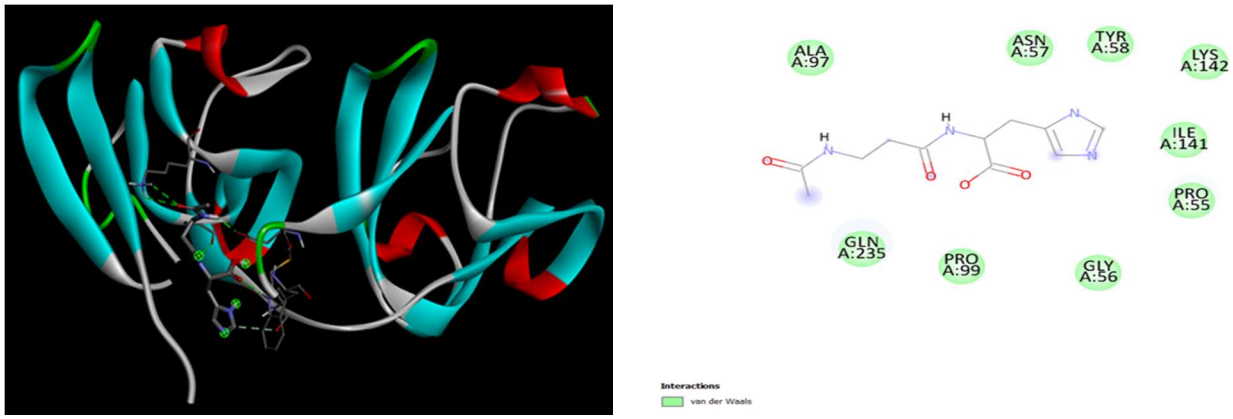

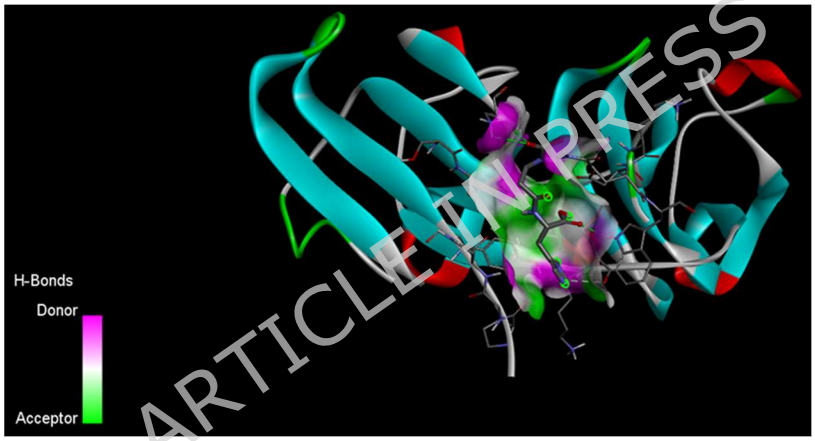

Figure 4. Molecular docking results of the ligand with Human βB1 Crystallin (PDB ID: 1OKI): (a) Docking pose of the ligand in the active site, (b) 2D representation of the ligand–protein interactions, and (c) hydrogen bond interaction map.

3. Strongest Interaction with γD-Crystallin (PDB: 1HK0)

Among all the analyzed targets, γD-crystallin exhibited the highest binding affinity with a docking score of −6.0 kcal/mol, accompanied by very short hydrogen bond distances (<2.0 Å), particularly with Tyr45 and Arg79. These residues are structurally important for maintaining the compact core stability of the lens. Notably, γD-crystallin is recognized as one of the most aggregation-prone crystallins during aging, where oxidative or thermal destabilization promotes protein unfolding and aggregate formation, leading to light scattering and cataract development. Therefore, stabilizing the native fold of γD-crystallin is considered a promising anti-cataract therapeutic strategy, as preventing its misfolding and aggregation may help preserve lens transparency (3, 27, 100, 101). As shown in Figure (5).

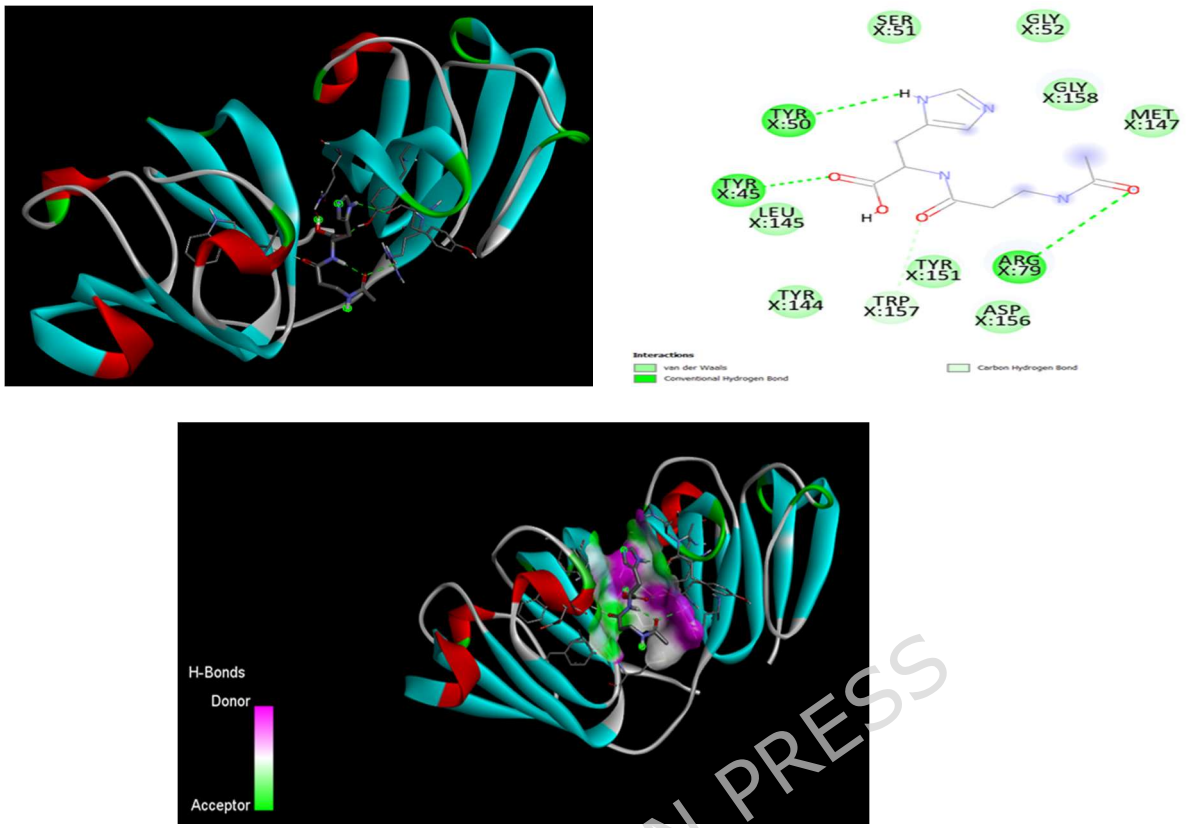

Figure 5. Molecular docking results of the ligand with Human GammaD Crystallin (PDB ID: 1HK0): (a) Docking pose of the ligand in the active site, (b) 2D representation of the ligand–protein interactions, and (c) hydrogen bond interaction map.

4. Interaction with Cystatin-C (PDB: 3GAX)

The ligand also formed multiple stabilizing interactions with Arg93, including hydrogen bonds and π–cation interactions, indicating a potential role in modulating protease-inhibition pathways. Notably, dysregulation of Cystatin-C is closely associated with amyloidogenic protein aggregation in several degenerative conditions. Therefore, these binding interactions suggest that the ligand may exert a broader protective effect by reducing pathological protein aggregation, extending beyond the maintenance of lens transparency alone(102). As shown in Figure (6).

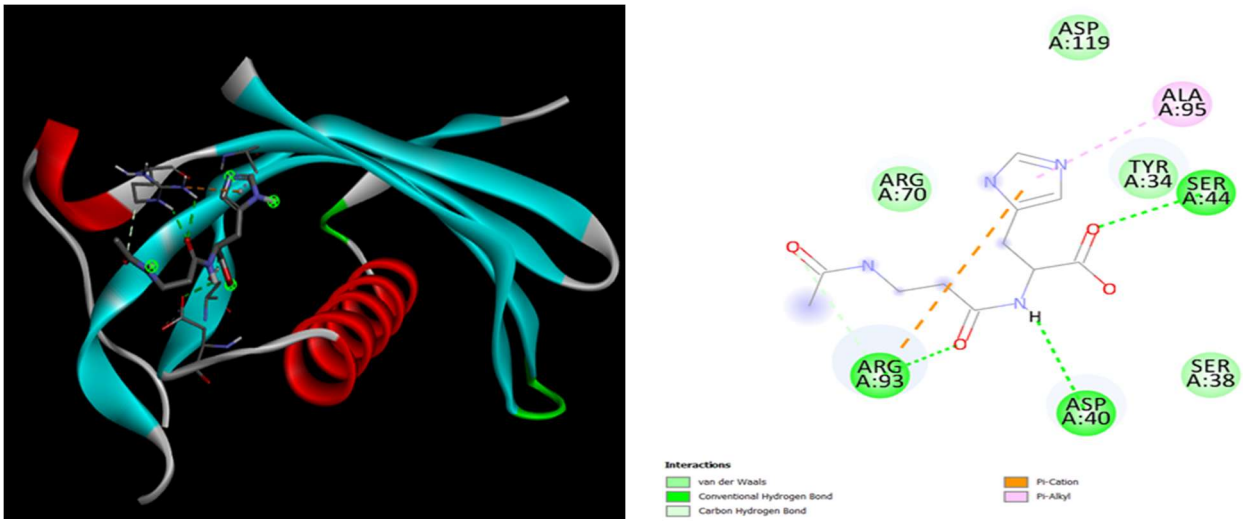

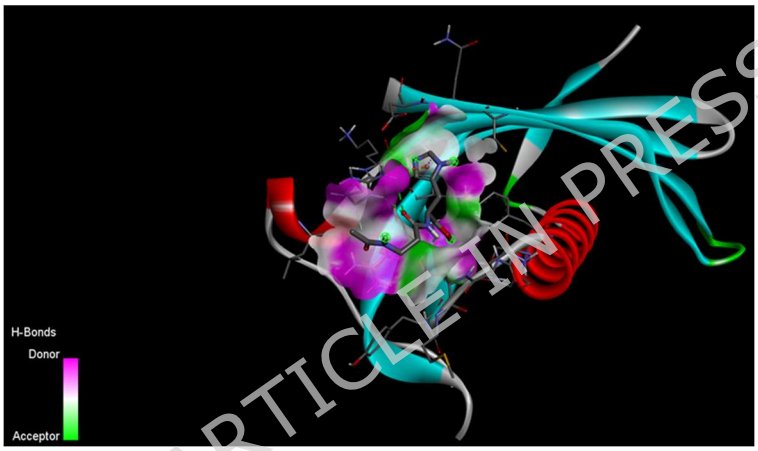

Figure 6. Molecular docking results of the ligand with Human Cystatin C (PDB ID: 3GAX): (a) Docking pose of the ligand in the active site, (b) 2D representation of the ligand–protein interactions, and (c) hydrogen bond interaction map.

Overall Interpretation

Collectively, the molecular docking results indicate that the ligand may function as a molecular stabilizer across several aggregation-sensitive crystallin proteins, through the formation of short-range hydrogen bonds, electrostatic interactions, and reinforcement of the native protein folding interfaces. Together, these interactions act to reduce protein aggregation and structural destabilization, thereby slowing the progression of lens opacity. Accordingly, the ligand may represent a candidate for further preclinical investigation in anti-cataract nanotherapeutic development.(102, 103). The detailed interaction distances between molecule and types are summarized in Table 2S.

ADMET study

Pharmacophore modeling of NAC revealed the presence of well-defined functional interaction features, including hydrogen-bond donor and acceptor sites, a negatively charged anionic region associated with the carboxylate group,

and hydrophobic interaction zones. These features, illustrated in Figure 4S(A), indicate the ligand's ability to engage in selective electrostatic and hydrophobic interactions with positively charged amino acid side chains located within biologically relevant protein binding pockets (28). The presence of complementary hydrogen-bonding motifs and anionic interaction centers suggests that NAC can stabilize protein structures by forming directional intermolecular networks with Crystallin residues, which are known to play a critical role in maintaining lens protein solubility and structural integrity (104). Furthermore, the hydrophobic domains identified in the Pharmacophore map support NAC's potential to interact with hydrophobic cores of Crystallin proteins, thereby reinforcing the native protein fold and reducing aggregation susceptibility under oxidative and thermal stress conditions—key mechanisms implicated in age-related cataract formation(105). Collectively, these Pharmacophore characteristics support the hypothesis that NAC can act as a molecular stabilizer, counteracting Crystallin unfolding and aggregation processes that drive age-related lens opacity, thereby positioning NAC as a promising therapeutic candidate for anti-cataract intervention (106).

NAC demonstrated favorable drug-like and therapeutic development properties, meeting the key absorption and systemic suitability criteria described by Lipinski, Veber, and Egan. According to SwissADME analysis, *In silico* predictions showed that NAC had good pharmacokinetic and drug-like properties, which means it would be a good candidate for further formulation development.(107). The BOILED-Egg predictive model, Figure 4S (B), further indicated that NAC does not cross the blood–brain barrier (BBB), a desirable characteristic for ophthalmic therapeutics, as lack of CNS penetration reduces the risk of neurological side effects and supports target-localized pharmacological action(108). Regarding safety, ProTox-II classification predicted NAC to possess low acute toxicity, with an estimated LD50 ≈ 14,930 mg/kg, and categorized it as non-carcinogenic, non-immunotoxic, and non-mutagenic, with only mild cardiotoxic and nephrotoxic potential observed at excessively high doses—consistent with its well-established safety record in ophthalmic formulations(54). Overall, these pharmacokinetic and toxicological characteristics support NAC as a clinically suitable, safe, and bioavailable therapeutic candidate, particularly for use in ocular drug delivery systems where localized antioxidant protection and minimal systemic side effects are essential. Table 3S. Predicted ADMET and Toxicity Profile of NAC.

Preparation of Human Cataract Lens Samples

Human cataractous lens specimens were obtained from patients undergoing routine cataract extraction surgeries due to diabetic-related or renal-failure–associated cataracts.

As shown in Figure 7, treatment resulted in a marked and progressive improvement in lens transparency over the course of 0 to 15 days following immersion in NAC at a concentration of 0.3 mM. A concurrent decrease in the yellowing intensity and overall opacity was observed when compared to the pre-treatment state of the samples derived from both diabetic and renal-failure cataract patients. This improvement is attributable to the ability of carnosine-derived compounds to combat protein aggregation, inhibit the formation of advanced glycation end products (AGEs) and reduce oxidative stress (104). In the case of lenses from renal-failure-associated cataracts, opacity is driven largely by elevated oxidative stress and ureamic toxins, whereas in diabetic-associated cataracts the activation of the polyol

pathway, accumulation of AGEs and associated oxidative/osmotic stress lead to lens protein damage and clouding (109). When 0.05 mM NAC was loaded onto AuNPs, a slight but noticeable enhancement in lens transparency was observed as shown in Figure (7). Such a low NAC dose may be insufficient to effectively counteract protein aggregation within the lens matrix, despite the known ability of AuNPs to facilitate localized drug delivery and prolonged retention at the target site (34). Gold nanoparticles are recognized for their ability to enhance tissue permeability, extend ocular residence time, and provide controlled and sustained drug release, all of which collectively contribute to improved bioavailability and therapeutic efficacy. Moreover, there was no spectral interference between the surface plasmon resonance (SPR) peak of gold nanoparticles (~520 nm) and the characteristic absorption of NAC (220 nm), ensuring accurate monitoring of both components within the composite formulation (110).

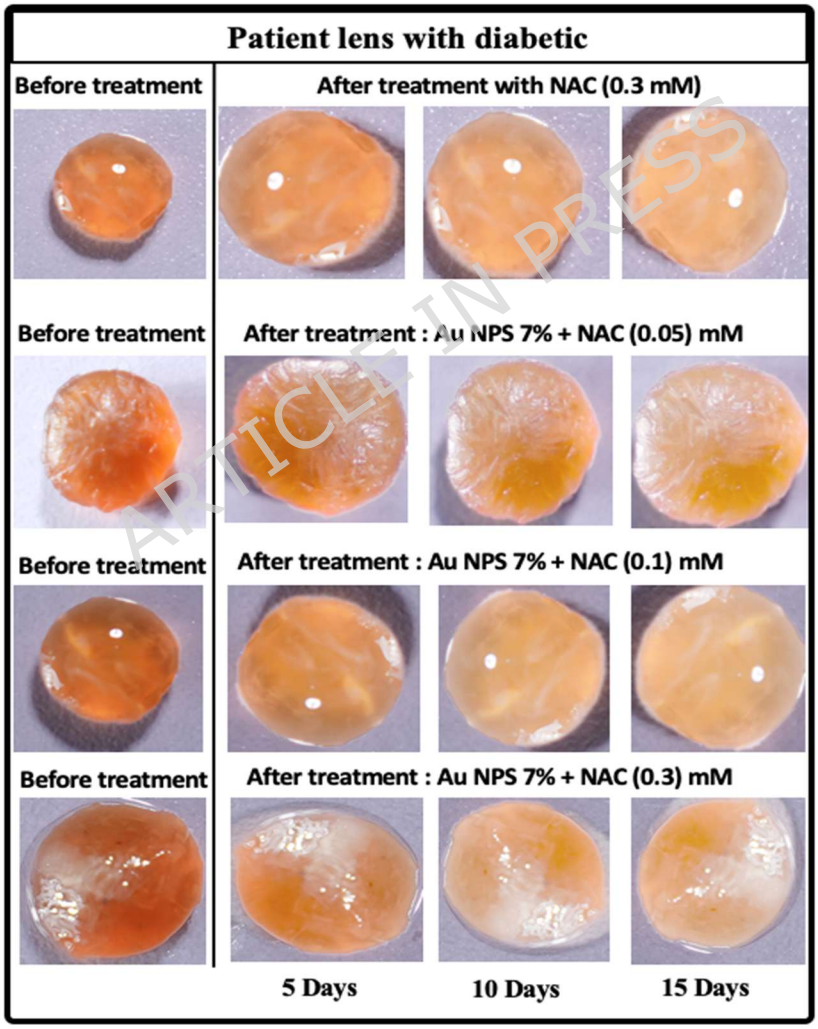

Figure 7. *Ex vivo* human lenses for diabetic patients treated with AuNPs (7%) and different concentrations of NAC (0.05, 0.1, 0.3 mM) over time-course (0, 5, 10, 15 days).

As illustrated in Figure 7, a marked improvement in lens transparency was observed between Days 10 and 15 compared to the lower concentration group. This finding indicates a dose-dependent therapeutic response, wherein increasing the NAC concentration to 0.1 mM, in the presence of AuNPs. Figure 8. *Ex vivo* human lenses for renal failure patients treated with AuNPs (7%) and different concentrations of NAC (0.05, 0.1, 0.3 mM) over time-course (0, 5, 10, 15 days).

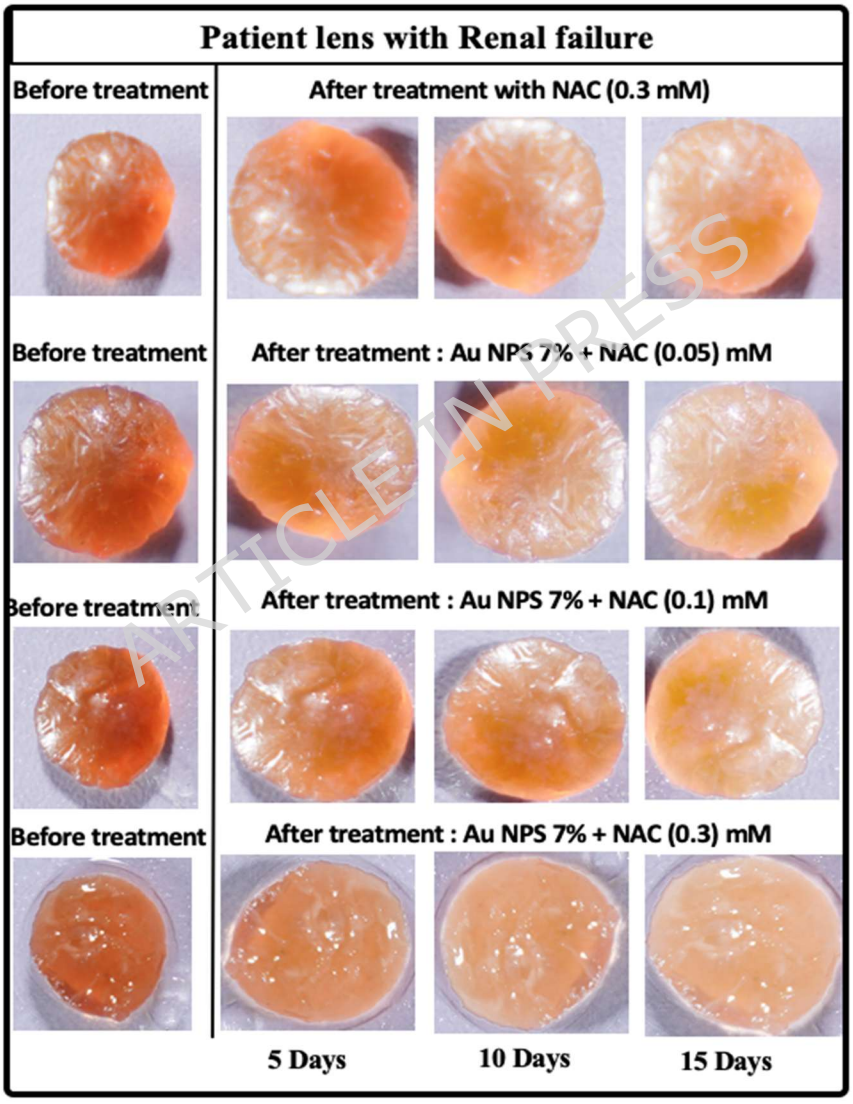

Figure 8. *Ex vivo* human lenses for renal patients treated with AuNPs (7%) and different concentrations of NAC (0.05, 0.1, 0.3 mM) over time-course (0, 5, 10, 15 days).

Advanced glycation end products (AGEs) are recognized as central pathological mechanisms underlying lens opacity in diabetes and chronic renal failure. Therefore, the improved lens clarity at 0.1 mM NAC aligns with recent evidence highlighting the ability of antioxidant and antiglycation compounds to preserve lens proteins and delay cataract progression through redox balance restoration and inhibition of AGE cross-linking (133).

A pronounced and qualitative improvement in lens transparency was observed during Days 10–15 compared to the lower NAC concentrations. A notable reduction in darkened regions and a more homogeneous optical appearance were evident, supporting the hypothesis that increasing the therapeutic dose in conjunction with AuNPs-based delivery effectively enhances the intralenticular bioavailability of NAC (111). This synergy promotes the dispersion of aggregated proteins and the sustained inhibition of glycation and oxidative processes within the lens tissue (112). These results are consistent with recent reports suggesting a potential synergistic effect of higher NAC loading that nanocarrier-assisted ocular drug delivery systems significantly improve drug permeability, ocular retention, and targeted release kinetics, thereby maintaining effective drug levels in otherwise inaccessible ocular compartments (30). Indeed, conventional topical therapies typically deliver less than 1–5 % of the applied dose to intraocular tissues due to the restrictive corneal and tear-film barriers (113). The incorporation of AuNP-based nanocarriers may offer a strategy to improve ocular drug retention and controlled release. (114).

Limitations of the study

There are some limitations to the current study. The *ex vivo* human lens model offers significant translational insights into the restoration of lens transparency; however, it does not completely emulate the dynamic physiological conditions of the living eye. Longer incubation times and pH levels that are relevant to physiology were used to partially make up for this problem. Additionally, the accessibility and management of human cataractous lenses presented technical difficulties, as lens tissues are extremely susceptible to mechanical and biochemical stress, which could compromise tissue integrity during storage and processing. The biological assessment was limited to *in vitro* (DPPH and MTT) and *ex vivo* models, which are insufficient to accurately predict *in vivo* pharmacokinetics, tissue penetration, or long-term safety. Furthermore, computational docking and ADMET analyses continue to be predictive and necessitate experimental validation. Consequently, extensive *in vivo* investigations are essential to validate therapeutic efficacy, biodistribution, and long-term biosafety prior to clinical application.

Conclusions

This study developed and characterized a green-synthesized AuNPs utilizing *Alchemilla vulgaris L* extract as a natural reducing and stabilizing agent for the administration of N-acetylcarnosine (NAC). The NAC-loaded AuNPs (crystalline size ranged between 20–35 nm) showed good physical and chemical properties, encapsulation efficiency, and good antioxidant activity. The findings suggest potential applicability in addressing oxidative stress–related lens alterations associated with cataractogenesis. The cytocompatibility of AuNPs-NAC formula against Human lens epithelial cells (HLE-B3) maintained acceptable cytocompatibility levels in HLE-B3 cells. *Ex vivo* human lens experiments showed a concentration-dependent improvement in lens optical clarity in both diabetic and renal failure–

associated cataract models. To the best of our knowledge, this study provides preliminary *ex vivo* evidence supporting the potential application of green-synthesized AuNPs-NAC formulations for further translational investigation in cataract management. Molecular docking and ADMET analyses provided supportive mechanistic and safety insights into the molecular stabilization of lens crystallin proteins and validated the advantageous safety profile of NAC. The results suggest that NAC-loaded AuNPs. Could be a possible non-surgical nanotherapeutic approach for reducing oxidative stress-related cataract formation and improving the efficiency of ocular drug delivery, but more *in vivo* testing is needed.

Acknowledgment

This work was a PhD project for Ahmed which issued in 2024. Deep appreciation is also extended to the staff of Ibn Al-Haitham Teaching Eye Hospital - Ministry of Health (Baghdad, Iraq), for their generous cooperation in providing human cataractous lens samples and facilitating the *ex vivo* experimental procedures. The authors further extend profound thanks to the Department of Chemistry, College of Science, Mustansiriyah University, for their technical support and assistance.

Declarations:

-Funding: This work received no funds.

-Availability of Data and Material: The authors declare that the data supporting the findings of this study are available within the paper and its supplementary information file.

-Conflict of Interests: No conflict of interest needs to be declared.

-**Ethics declaration**: The Institutional Ethics Committee of Ibn Al-Haitham Teaching Eye Hospital – Minsitry of Health in Baghdad, Iraq, reviewed and approved all experimental protocols that used samples of human cataractous lenses. The study adhered to the ethical guidelines outlined in the Declaration of Helsinki, and written informed consent was secured from all participants prior to sample collection. The College of Science Ethics committee in Mustansiriyah University approved the study proposal. This Ethics committee is working in accordance to College of Science guidelines on biomedical research. Ref. BCSMU/0225/00020C.None of the Investigator and co-investigator participating in this study took part in the decision making and voting procedure for this study. The College of Science`s Scientific committee expects to be informed about the progress of the study, any serious adverse events occurring in the course of the study, and any revision in the protocol.

-**Author Contributions: Ahmed Salih Abid** performed the lab work, interpreted the results, wrote the first draft, edited it, and authorized the final draft. **Zahraa S. Al-Garawi** designed the study, supervised the whole project, interpreted the results, participated in writing the first and final version, edited and authorized the final version. **Füreya Elif Öztürkkan** performed the computerized and theoretical study, participated in writing the first and final version, edited and authorized the final version.

AI-Assisted Language Editing Statement

The authors enhanced the manuscript's grammar, readability, and clarity by using AI-based language editing tools (ChatGPT, OpenAI).

References

1. Chen SP, Woreta F, Chang DF. Cataracts: a review. JAMA. 2025.
2. Study VLEGotGBoD. Global estimates on the number of people blind or visually impaired by cataract: a meta-analysis from 2000 to 2020. Eye. 2024;38(11):2156.
3. Loh D, Reiter RJ. β/γ-Crystallins, Redox Chemistry, and Melatonin: The Regulation of Phase Separation in Cataractogenesis. 2025.
4. Zhang M, Zhang R, Zhao X, Ma Z, Xin J, Xu S, et al. The role of oxidative stress in the pathogenesis of ocular diseases: An overview. Molecular Biology Reports. 2024;51(1):454.
5. Nadeem S. Cataract surgery: historical devices, modern innovations, and future perspectives. Taylor & Francis; 2024. p. 991-4.
6. Durgapal S, Kumar P, Pandey BS, Das J, Sridhar SB, Ashique S, et al. Cataract Management in the Modern Era: Therapeutic Advances and Unmet Needs. Current Pharmaceutical Design. 2025.
7. Díez-Pascual AM. Surface engineering of nanomaterials with polymers, biomolecules, and small ligands for nanomedicine. Materials. 2022;15(9):3251.
8. Nasraty N. Investigating the Role of The Antioxidant N-acetylcarnosine in Attenuating Oxidation-induced Retinal Damage in Retinitis Pigmentosa: Harvard University; 2021.
9. Dammak A, Pastrana C, Martin-Gil A, Carpena-Torres C, Peral Cerda A, Simovart M, et al. Oxidative stress in the anterior ocular diseases: diagnostic and treatment. Biomedicines. 2023;11(2):292.
10. Wang Y, Cao K, Guo Z-X, Wan X-H. Effect of lens crystallins aggregation on cataract formation. Experimental Eye Research. 2025:110288.
11. Butt A, Bach H. Advancements in nanotechnology for diagnostics: a literature review, part II: advanced techniques in nuclear and optical imaging. Nanomedicine. 2025;20(2):183-206.
12. Gupta PC, Sharma N, Mishra P, Rai S, Verma T. Role of gold nanoparticles for targeted drug delivery. Metal and Metal-Oxide Based Nanomaterials: Synthesis, Agricultural, Biomedical and Environmental Interventions: Springer; 2024. p. 243-69.
13. Hang Y, Wang A, Wu N. Plasmonic silver and gold nanoparticles: shape-and structure-modulated plasmonic functionality for point-of-caring sensing, bio-imaging and medical therapy. Chemical Society Reviews. 2024;53(6):2932-71.
14. Babizhayev MA. Ocular drug metabolism of the bioactivating antioxidant N-acetylcarnosine for vision in ophthalmic prodrug and codrug design and delivery. Drug development and industrial pharmacy. 2008;34(10):1071-89.
15. Georgeous J, AlSawaftah N, Abuwatfa WH, Husseini GA. Review of gold nanoparticles: synthesis, properties, shapes, cellular uptake, targeting, release mechanisms and applications in drug delivery and therapy. Pharmaceutics. 2024;16(10):1332.
16. Gul M, Kashif M, Muhammad S, Azizi S, Sun H. Various Methods of Synthesis and Applications of Gold-Based Nanomaterials: A Detailed Review. Crystal Growth & Design. 2025;25(7):2227-66.
17. Rosero WAA, Barbezan AB, de Souza CD, Rostelato MECM. Review of advances in coating and functionalization of gold nanoparticles: from theory to biomedical application. Pharmaceutics. 2024;16(2):255.
18. Zhang W, Taheri-Ledari R, Ganjali F, Afruzi FH, Hajizadeh Z, Saeidirad M, et al. Nanoscale bioconjugates: A review of the structural attributes of drug-loaded nanocarrier conjugates for selective cancer therapy. Heliyon. 2022;8(6).
19. Giri BR, Jakka D, Sandoval MA, Kulkarni VR, Bao Q. Advancements in ocular therapy: a review of emerging drug delivery approaches and pharmaceutical technologies. Pharmaceutics. 2024;16(10):1325.
20. Lanier OL, Manfre MG, Bailey C, Liu Z, Sparks Z, Kulkarni S, et al. Review of approaches for increasing ophthalmic bioavailability for eye drop formulations. Aaps Pharmscitech. 2021;22(3):107.
21. Račić A, Krajišnik D. Biopolymers in mucoadhesive eye drops for treatment of dry eye and allergic conditions: application and perspectives. Pharmaceutics. 2023;15(2):470.

22. Gabai A, Zeppieri M, Finocchio L, Salati C. Innovative strategies for drug delivery to the ocular posterior segment. Pharmaceutics. 2023;15(7):1862.
23. Rykowska I, Nowak I, Nowak R. Soft contact lenses as drug delivery systems: a review. Molecules. 2021;26(18):5577.
24. Liu Y, Wu N. Progress of nanotechnology in diabetic retinopathy treatment. International journal of nanomedicine. 2021:1391-403.
25. Ko W-C, Wang S-J, Hsiao C-Y, Hung C-T, Hsu Y-J, Chang D-C, et al. Pharmacological role of functionalized gold nanoparticles in disease applications. Molecules. 2022;27(5):1551.
26. Watchorn J, Clasky AJ, Prakash G, Johnston IA, Chen PZ, Gu FX. Untangling mucosal drug delivery: engineering, designing, and testing nanoparticles to overcome the mucus barrier. ACS biomaterials science & engineering. 2022;8(4):1396-426.
27. Budnar P, Tangirala R, Bakthisaran R, Rao CM. Protein aggregation and cataract: role of age-related modifications and mutations in α-crystallins. Biochemistry (Moscow). 2022;87(3):225-41.
28. Anwar S, Khan S, Almatroudi A, Khan AA, Alsahli MA, Almatroodi SA, et al. A review on mechanism of inhibition of advanced glycation end products formation by plant derived polyphenolic compounds. Molecular Biology Reports. 2021;48(1):787-805.
29. Rodella U, Honisch C, Gatto C, Ruzza P, D'Amato Tóthová J. Antioxidant nutraceutical strategies in the prevention of oxidative stress related eye diseases. Nutrients. 2023;15(10):2283.
30. Li S, Chen L, Fu Y. Nanotechnology-based ocular drug delivery systems: recent advances and future prospects. Journal of nanobiotechnology. 2023;21(1):232.
31. Santos G, Delgado E, Silva B, Braz BS, Gonçalves L. Topical Ocular Drug Delivery: The Impact of Permeation Enhancers. Pharmaceutics. 2025;17(4):447.
32. Raîche-Marcoux G, Méthot S, Tchatchouang A, Bettoli C, Maranda C, Loiseau A, et al. Localization of fluorescent gold nanoparticles throughout the eye after topical administration. Frontiers in Medicine. 2025;12:1557611.
33. Rai A, Ferreira L. Biomedical applications of the peptide decorated gold nanoparticles. Critical Reviews in Biotechnology. 2021;41(2):186-215.
34. Chen Y, Ye Z, Chen H, Li Z. Breaking barriers: nanomedicine-based drug delivery for cataract treatment. International Journal of Nanomedicine. 2024:4021-40.
35. Qi M, Tay A. Phage–nanomaterial platforms for precision antimicrobial therapy: from design to therapeutic application. Nanoscale. 2025.
36. Bilušić T, Šola I, Čikeš Čulić V. Identification of Flavonoids, Antioxidant and Antiproliferative Activity of Aqueous Infusions of Calendula officinalis L., Chelidonium majus L., Teucrium chamaedrys L. and Alchemilla vulgaris L. Food technology and biotechnology. 2024;62(1):49-58.
37. Abdulsada TN, Rheima AM, Al-Rubae'i SH. Sustainable new biosynthesis of Zero valence gold nanoparticles via Healthy Alchemilla vulgaris L. extract as capping agent. Case Studies in Chemical and Environmental Engineering. 2024;10:100888.
38. Parramon JS, Švarc T, Majerič P, Jelen Ž, Rudolf R. Optical Characteristics of Directly Deposited Gold Nanoparticle Films. Surfaces. 2024;7(2):369-79.
39. Mradu G, Saumyakanti S, Sohini M, Arup M. HPLC profiles of standard phenolic compounds present in medicinal plants. International Journal of Pharmacognosy and Phytochemical Research. 2012;4(3):162-7.
40. Pasieczna-Patkowska S, Cichy M, Flieger J. Application of Fourier transform infrared (FTIR) spectroscopy in characterization of green synthesized nanoparticles. Molecules. 2025;30(3):684.
41. Pechyen C, Ponsanti K, Tangnorawich B, Ngernyuang N. Biogenic synthesis of gold nanoparticles mediated by Spondias dulcis (Anacardiaceae) peel extract and its cytotoxic activity in human breast cancer cell. Toxicology Reports. 2022;9:1092-8.

42. Thongwattana T, Chaiyo R, Ponsanti K, Tangnorawich B, Pratumpong P, Toommee S, et al. Synthesis of Silver Nanoparticles and Gold Nanoparticles Used as Biosensors for the Detection of Human Serum Albumin-Diagnosed Kidney Disease. Pharmaceuticals. 2024;17(11):1421.
43. Farkas S, Holló G, Schuszter G, Deák Á, Janovák L, Hornok V, et al. Reaction–diffusion assisted synthesis of gold nanoparticles: Route from the spherical nano-sized particles to micrometer-sized plates. The Journal of Physical Chemistry C. 2021;125(47):26116-24.
44. Gorohovs M, Dekhtyar Y. Surface Functionalization of Nanoparticles for Enhanced Electrostatic Adsorption of Biomolecules. Molecules. 2025;30(15):3206.
45. Lopes J, Ferreira-Gonçalves T, Ascensao L, Viana A, Carvalho L, Catarino J, et al. Safety of gold nanoparticles: from in vitro to in vivo testing array checklist, Pharmaceutics 15 (2023) 1120.
46. Raiche-Marcoux G, Loiseau A, Maranda C, Poliquin A, Boisselier E. Parametric drug release optimization of anti-inflammatory drugs by gold nanoparticles for topically applied ocular therapy. International Journal of Molecular Sciences. 2022;23(24):16191.
47. Wang J, Giordani S, Marassi V, Placci A, Roda B, Reschiglian P, et al. Multi-environment and multi-parameter screening of stability and coating efficiency of gold nanoparticle bioconjugates in application media. Scientific Reports. 2024;14(1):31568.
48. de Diego-García L, Rejas-González R, Latre IC, Guzman-Aranguez A. Pharmacological Strategies for Cataract Management: From Molecular Targets to Clinical Translation. International Journal of Molecular Sciences. 2025;26(12):5658.
49. Kim H-M, Park JH, Choi YJ, Oh J-M, Park J. Hyaluronic acid-coated gold nanoparticles as a controlled drug delivery system for poorly water-soluble drugs. RSC advances. 2023;13(8):5529-37.
50. Seegobin N, McCoubrey LE, Vignal C, Waxin C, Abdalla Y, Fan Y, et al. Dual action tofacitinib-loaded PLGA nanoparticles alleviate colitis in an IBD mouse model. Drug delivery and translational research. 2025;15(7):2372-89.
51. Budama-Kilinc Y, Cakir-Koc R, Kecel-Gunduz S, Kokcu Y, Bicak B, Mutlu H, et al. Novel NAC-loaded poly (lactide-co-glycolide acid) nanoparticles for cataract treatment: preparation, characterization, evaluation of structure, cytotoxicity, and molecular docking studies. PeerJ. 2018;6:e4270.
52. Sunseri J, Koes DR. Pharmit: interactive exploration of chemical space. Nucleic acids research. 2016;44(W1):W442-W8.
53. Daina A, Michielin O, Zoete V. SwissADME: a free web tool to evaluate pharmacokinetics, drug-likeness and medicinal chemistry friendliness of small molecules. Scientific reports. 2017;7(1):42717.
54. Banerjee P, Kemmler E, Dunkel M, Preissner R. ProTox 3.0: a webserver for the prediction of toxicity of chemicals. Nucleic Acids Research. 2024;52(W1):W513-W20.
55. Trott O, Olson AJ. AutoDock Vina: improving the speed and accuracy of docking with a new scoring function, efficient optimization, and multithreading. Journal of computational chemistry. 2010;31(2):455-61.
56. Du J, Singh H, Dong W-j, Bai Y-h, Yi T-H. Colorimetric detection of Listeria monocytogenes using one-pot biosynthesized flower-shaped gold nanoparticles. Sensors and Actuators B: Chemical. 2018;265:285-92.
57. Bharadwaj KK, Rabha B, Pati S, Sarkar T, Choudhury BK, Barman A, et al. Green synthesis of gold nanoparticles using plant extracts as beneficial prospect for cancer theranostics. Molecules. 2021;26(21):6389.
58. Fathalla Z, Mustafa WW, Abdelkader H, Moharram H, Sabry AM, Alany RG. Hybrid thermosensitive-mucoadhesive in situ forming gels for enhanced corneal wound healing effect of L-carnosine. Drug delivery. 2022;29(1):374-85.

59. Wang Y, Xia R, Hu H, Peng T. Biosynthesis, characterization and cytotoxicity of gold nanoparticles and their loading with N-acetylcarnosine for cataract treatment. Journal of Photochemistry and Photobiology B: Biology. 2018;187:180-3.
60. Botteon CEA, Silva LB, Ccana-Ccapatinta GV, Silva T, Ambrosio SR, Veneziani R, et al. Biosynthesis and characterization of gold nanoparticles using Brazilian red propolis and evaluation of its antimicrobial and anticancer activities. Scientific Reports. 2021;11(1):1974.
61. Wang L, Liu W, Huang X. An approach to revolutionize cataract treatment by enhancing drug probing through intraocular cell line. Libyan Journal of Medicine. 2018;13(1).
62. Muddapur UM, Alshehri S, Ghoneim MM, Mahnashi MH, Alshahrani MA, Khan AA, et al. Plant-based synthesis of gold nanoparticles and theranostic applications: a review. Molecules. 2022;27(4):1391.
63. Sharma R, Yadav A, Arora S, Kishore N. To study the structural properties of cobalt doped tin oxide nanostructured by using Williamson-Hall and size-strain plot methodology. Materials today: PROCEEDINGS. 2021;44:4651-6.
64. Adnan R. Gold-based Nanomaterials: Spectroscopy, Microscopy and Applications in Catalysis and Sensing. 2015.
65. Lin Z, Niu L, Zhang H, Shen H, Hu W, GUO F. Biosynthesis, optimization, and multifunctional biomedical applications of gold nanoparticles mediated by Streptomyces sp. YJD18. Frontiers in Microbiology. 2025;16:1667928.
66. Das B, Lou-Franco J, Gilbride B, Ellis MG, Stewart LD, Grant IR, et al. Peroxidase-mimicking activity of biogenic gold nanoparticles produced from Prunus nepalensis fruit extract: Characterizations and application for the detection of Mycobacterium bovis. ACS Applied Bio Materials. 2022;5(6):2712-25.
67. Kusuma SAF, Harmonis JA, Pratiwi R, Hasanah AN. Gold nanoparticle-based colorimetric sensors: properties and application in detection of heavy metals and biological molecules. Sensors. 2023;23(19):8172.
68. Al-Radadi NS, Al-Bishri WM, Salem NA, ElShebiney SA. Plant-mediated green synthesis of gold nanoparticles using an aqueous extract of Passiflora ligularis, optimization, characterizations, and their neuroprotective effect on propionic acid-induced autism in Wistar rats. Saudi Pharmaceutical Journal. 2024;32(2):101921.
69. Huang X, Devi S, Bordiga M, Brennan CS, Xu B. Phenolic compounds mediated biosynthesis of gold nanoparticles and evaluation of their bioactivities: a review. International Journal of Food Science and Technology. 2023;58(4):1673-94.
70. Kahraman HT. Synthesis of silver nanoparticles using Alchemilla vulgaris and Helichrysum arenarium for methylene blue and 4-nitrophenol degradation and antibacterial applications. Biomass Conversion and Biorefinery. 2024;14(12):13479-90.
71. Usman M, Ishafaq M, Muhammad Z, Ali W, Dastgeer G, Zhang X, et al. Evaporation-induced self-assembly of gold nanorods on a hydrophobic substrate for surface enhanced Raman spectroscopy applications. Frontiers in Materials. 2023;9:1048011.
72. Panchal P, Rauwel P, Nehra SP, Singh P, Karla M, Hermosa G, et al. A Review on Biomedical Applications of Plant Extract-Mediated Metallic Ag, Au, and ZnO Nanoparticles and Future Prospects for Their Combination with Graphitic Carbon Nitride. Pharmaceuticals. 2025;18(6):820.
73. Holišová V, Urban M, Konvičková Z, Kolenčík M, Mančík P, Slabotinský J, et al. Colloidal stability of phytosynthesised gold nanoparticles and their catalytic effects for nerve agent degradation. Sci Rep 11: 1–9. 2021.
74. Nisha, Sachan RSK, Singh A, Karnwal A, Shidiki A, Kumar G. Plant-mediated gold nanoparticles in cancer therapy: Exploring anti-cancer mechanisms, drug delivery applications, and future prospects. Frontiers in Nanotechnology. 2024;6:1490980.

75. Chonanant C, Maraming P, Daduang J, Limpaiboon T, Prakrankamanant P, Ngernyuang N. Green synthesis of biocompatible gold nanoparticles using andrographis paniculata leaves extract for targeted detection of human epidermal growth factor receptor 2-Positive breast cancer cells. ACS Organic & Inorganic Au. 2025;5(5):328-37.
76. Bilardo R, Traldi F, Vdovchenko A, Resmini M. Influence of surface chemistry and morphology of nanoparticles on protein corona formation. Wiley Interdisciplinary Reviews: Nanomedicine and Nanobiotechnology. 2022;14(4):e1788.
77. Uritu CM, Al-Matarneh CM, Bostiog DI, Coroaba A, Ghizdovat V, Filipiuc SI, et al. Radiolabeled multi-layered coated gold nanoparticles as potential biocompatible PET/SPECT tracers. Journal of Materials Chemistry B. 2024;12(15):3659-75.
78. Hussain MH, Abu Bakar NF, Mustapa AN, Low K-F, Othman NH, Adam F. Synthesis of various size gold nanoparticles by chemical reduction method with different solvent polarity. Nanoscale research letters. 2020;15(1):140.
79. Leach R. Characterisation of areal surface texture: Springer; 2013.
80. Lipa Z, Tomanícková D. Utilisation of abbott-firestone curves characteristics for the determination of turned surface properties. Annals of the Faculty of Engineering Hunedoara. 2011;9(3):223.
81. Tukova A, Tavakkoli Yaraki M, Rodger A, Wang Y. Shape-induced variations in aromatic thiols adsorption on gold nanoparticle: a novel method for accurate evaluation of adsorbed molecules. Langmuir. 2023;39(44):15828-36.
82. Yang Y, Knust S, Schwiderek S, Qin Q, Yun Q, Grundmeier G, et al. Protein adsorption at nanorough titanium oxide surfaces: The importance of surface statistical parameters beyond surface roughness. Nanomaterials. 2021;11(2):357.
83. Adamczyk Z, Sadowska M, Nattich-Rak M. Quantifying nanoparticle layer topography: Theoretical modeling and atomic force microscopy investigations. Langmuir. 2023;39(42):15067-77.
84. Mizzi L, Chatzitzika C, Gatt R, Valdramidis V. HPLC analysis of phenolic compounds and flavonoids with overlapping peaks. Food technology and biotechnology. 2020;58(1):12-9.
85. Irakli M, Skendi A, Bouloumpasi E, Chatzopoulou P, Biliaderis CG. LC-MS identification and quantification of phenolic compounds in solid residues from the essential oil industry. Antioxidants. 2021;10(12):2016.
86. Riss TL, Moravec RA, Niles AL, Duellman S, Benink HA, Worzella TJ, et al. Cell viability assays. Assay guidance manual [Internet]. 2016.
87. Gruber S, Nickel A. Toxic or not toxic? Interlaboratory comparison reveals almost fifty-fifty chance in the cytotoxicity assessment (ISO 10993-5) of an identical medical device. MedRxiv. 2023:2023.03. 28.23287847.
88. Jablonska E, Kubásek J, Vojtěch D, Ruml T, Lipov J. Test conditions can significantly affect the results of in vitro cytotoxicity testing of degradable metallic biomaterials. Scientific Reports. 2021;11(1):6628.
89. Pfaff A, Chernatynskaya A, Vineyard H, Ercal N. Thiol antioxidants protect human lens epithelial (HLE B-3) cells against tert-butyl hydroperoxide-induced oxidative damage and cytotoxicity. Biochemistry and Biophysics Reports. 2022;29:101213.
90. Kanak S, Krzemińska B, Celiński R, Bakalczuk M, Dos Santos Szewczyk K. Phenolic composition and antioxidant activity of Alchemilla species. Plants. 2022;11(20):2709.
91. Lee H-L, Chuang YC, Tsai J-T, Chen Y-C, Wu P-H, Lo L-W, et al. Gold nanodandelions as nanozymes and reactive oxygen species scavengers in tumor microenvironment components. ACS Applied Nano Materials. 2023;6(22):21359-70.

92. Dong Y, Chen Y, Zhu D, Shi K, Ma C, Zhang W, et al. Self-assembly of amphiphilic phospholipid peptide dendrimer-based nanovectors for effective delivery of siRNA therapeutics in prostate cancer therapy. Journal of Controlled Release. 2020;322:416-25.
93. Kanniyappan H, Jose J, Chakraborty S, Ramasamy M, Muthuvijayan V. pH-responsive drug release from positively charged mesoporous silica nanoparticles and their potential for anticancer drug delivery. Journal of the Australian Ceramic Society. 2023;59(1):207-20.
94. Sandaruwan HB, Manatunga DC, Liyanage RN, Costha NP, Dassanayake RS, Wijesinghe RE, et al. Next-generation methods for precise pH detection in ocular chemical burns: a review of recent analytical advancements. Analytical Methods. 2025;17(3):408-31.
95. Amrutkar CS, Patil SB. Nanocarriers for ocular drug delivery: recent advances and future opportunities. Indian Journal of Ophthalmology. 2023;71(6):2355-66.
96. Islam S, Do MT, Frank BS, Hom GL, Wheeler S, Fujioka H, et al. α-Crystallin chaperone mimetic drugs inhibit lens γ-crystallin aggregation: Potential role for cataract prevention. Journal of Biological Chemistry. 2022;298(10):102417.
97. Hill JA, Nyathi Y, Horrell S, von Stetten D, Axford D, Owen RL, et al. An ultraviolet-driven rescue pathway for oxidative stress to eye lens protein human gamma-D crystallin. Communications Chemistry. 2024;7(1):81.
98. Basak A, Bateman O, Slingsby C, Pande A, Asherie N, Ogun O, et al. High-resolution X-ray crystal structures of human γD crystallin (1.25 Å) and the R58H mutant (1.15 Å) associated with aculeiform cataract. Journal of molecular biology. 2003;328(5):1137-47.
99. Van Montfort RL, Bateman OA, Lubsen NH, Slingsby C. Crystal structure of truncated human βB1-crystallin. Protein Science. 2003;12(11):2606-12.
100. Andley UP. Crystallins in the eye: function and pathology. Progress in retinal and eye research. 2007;26(1):78-98.
101. Li H, Yu Y, Ruan M, Jiao F, Chen H, Gao J, et al. The mechanism for thermal-enhanced chaperone-like activity of α-crystallin against UV irradiation-induced aggregation of γD-crystallin. Biophysical journal. 2022;121(12):2233-50.
102. Kolodziejczyk R, Michalska K, Hernandez-Santoyo A, Wahlbom M, Grubb A, Jaskolski M. Crystal structure of human cystatin C stabilized against amyloid formation. The FEBS journal. 2010;277(7):1726-37.
103. Moreau KL, King JA. Protein misfolding and aggregation in cataract disease and prospects for prevention. Trends in molecular medicine. 2012;18(5):273-82.
104. Wang L, Li X, Men X, Liu X, Luo J. Research progress on antioxidants and protein aggregation inhibitors in cataract prevention and therapy. Molecular medicine reports. 2024;31(1):22.
105. Timsina R, Mainali L. Association of alpha-crystallin with fiber cell plasma membrane of the eye lens accompanied by light scattering and cataract formation. Membranes. 2021;11(6):447.
106. de Diego-García L, Rejas-González R, Latre IC, Guzman-Aranguez A. Pharmacological Strategies for Cataract Management: From Molecular Targets to Clinical Translation. International Journal of Molecular Sciences. 2025 Jun 13;26(12):5658.
107. Daina A, Michielin O, Zoete V. SwissADME: a free web tool to evaluate pharmacokinetics, drug-likeness and medicinal chemistry friendliness of small molecules. Scientific reports. 2017 Mar 3;7(1):42717.
108. Daina A, Zoete V. A boiled-egg to predict gastrointestinal absorption and brain penetration of small molecules. ChemMedChem. 2016;11(11):1117-21.
109. Chitra PS, Chaki D, Boiroju NK, Mokalla TR, Gadde AK, Agraharam SG, et al. Status of oxidative stress markers, advanced glycation index, and polyol pathway in age-related cataract subjects with and without diabetes. Experimental eye research. 2020;200:108230.

110. Ahmed S, Amin MM, Sayed S. Ocular drug delivery: a comprehensive review. AAPS PharmSciTech. 2023;24(2):66.
111. Masse F, Ouellette M, Lamoureux G, Boisselier E. Gold nanoparticles in ophthalmology. Medicinal research reviews. 2019;39(1):302-27.
112. Guo Z, Ma X, Zhang RX, Yan H. Oxidative stress, epigenetic regulation and pathological processes of lens epithelial cells underlying diabetic cataract. Advances in ophthalmology practice and research. 2023;3(4):180-6.
113. Souza JG, Dias K, Pereira TA, Bernardi DS, Lopez RF. Topical delivery of ocular therapeutics: carrier systems and physical methods. Journal of Pharmacy and Pharmacology. 2014;66(4):507-30.
114. F Fangueiro J, Veiga F, M Silva A, B Souto E. Ocular drug delivery-new strategies for targeting anterior and posterior segments of the eye. Current pharmaceutical design. 2016;22(9):1135-46.